



ACADÉMIE  
DES SCIENCES  
INSTITUT DE FRANCE

# *Comptes Rendus*

---

## *Géoscience*

### *Sciences de la Planète*

Serge Lallemand, Michel Peyret, Diane Arcay and Arnauld Heuret


**Accretion versus erosion and sediment transfer balance near the subduction interface**

Published online: 3 April 2024

**Part of Special Issue:** Geodynamics of Continents and Oceans – A tribute to Jean Aubouin

**Guest editors:** Olivier Fabbri (Université de Franche-Comté, UMR CNRS 6249, Besançon), Michel Faure (Université d'Orléans-BRGM, UMR CNRS 7325, Institut des Sciences de la Terre, Orléans), Jacky Ferrière (Université de Lille, faculté des Sciences), Laurent Jolivet (Sorbonne Université, IStEP, UMR 7193, Paris) and Sylvie Leroy (Sorbonne Université, CNRS-INSU, IStEP, Paris)

<https://doi.org/10.5802/crgeos.252>

 This article is licensed under the  
CREATIVE COMMONS ATTRIBUTION 4.0 INTERNATIONAL LICENSE.  
<http://creativecommons.org/licenses/by/4.0/>



*The Comptes Rendus. Géoscience — Sciences de la Planète are a member of the  
Mersenne Center for open scientific publishing*  
[www.centre-mersenne.org](http://www.centre-mersenne.org) — e-ISSN : 1778-7025



Research article

Geodynamics of Continents and Oceans – A tribute to Jean Aubouin

# Accretion versus erosion and sediment transfer balance near the subduction interface

Serge Lallemand<sup>\*,a</sup>, Michel Peyret<sup>\*,a</sup>, Diane Arcay<sup>\*,a</sup> and Arnaud Heuret<sup>\*,b</sup>

<sup>a</sup> Geosciences Montpellier, CNRS, Université de Montpellier, Université des Antilles, France

<sup>b</sup> Geosciences Montpellier, CNRS, Université de Montpellier, Université des Antilles, Université de Guyane, France

E-mail: [serge.lallemand@umontpellier.fr](mailto:serge.lallemand@umontpellier.fr) (S. Lallemand)

**Abstract.** The nature and amount of sediment transferred from one plate to the other near the subduction interface partly determines the tectonic and seismogenic regime of a margin. Examination of over 500 multichannel seismic lines has enabled us to build up a global database of subduction zone front characteristics at unprecedented spatial resolution. The total thickness of sediment in the trench below the deformation front, as well as that of the subduction channel at a distance from the trench, combined with other indices such as the tectonic regime of the forearc or the migration of the volcanic front, have enabled us to revisit the accretionary or erosional character of active margins. Preliminary conclusions, based on ~3/4 of sufficiently documented subduction zones, show a predominance of the erosive character of subduction over the last million years. The flux of solid matter through the shallow part of the subduction channel is of the order of 1.5 km<sup>3</sup>/yr, and that of pore fluids 0.4 km<sup>3</sup>/yr. Some subduction zones, such as the Mediterranean, are characterized by exceptional solid flux in the channel, while fluid flux is comparatively moderate. This is due to the fact that channel sediments are compacted even before subduction. Overall, fluid flux in the channel is greater under erosive margins, due to the higher rate of subduction and often higher porosity. Maximum porosity in the channel is reached when there is neither accretion nor tectonic erosion.

**Keywords.** Subduction, Active margins, Oceanic trenches, Subduction channel, Accretion, Erosion, Sediment flux.

*Manuscript received 5 July 2023, revised 20 November 2023, accepted 21 December 2023.*

## 1. Introduction

The existence of erosive processes responsible for the destruction of some active margins was first considered in the early 1970s along the Chilean subduction based on a mass balance deficit between sediment inputs from the Andes and those actually observed along the margin and in the trench [Scholl et al.,

1970], as well as a distribution of plutons showing an eastward rejuvenation from Jurassic in the coast to Cenozoic in the Cordillera [Rutland, 1971]. A little later, deep ocean drilling on active margins in Central America, the Marianas, Japan, or Peru provided additional support for the tectonic erosion process that explained both the anomalous subsidence of these margins (not explained by thermal contraction or sediment loading) and the landward migration of the volcanic front [Moore et al., 1986, Natland and Tarney, 1981, Bloomer, 1983, von Huene

\* Corresponding author.

et al., 1982, Suess et al., 1988]. These findings have challenged the established model of active margin growth by sediment accretion at the foot of the landward slope [e.g., Seely, 1979]. Aubouin et al. [1984, 1985], following an exploration of the Guatemalan margin [von Huene and Aubouin, 1982], introduced the concept of convergent-extensional margin, reflecting that many active margins are cut by normal faults as in passive margins [see also Ferrière and Faure, 2024]. Proposals to classify active margins on the basis of their accretionary or erosive characteristics have emerged since the 1990s as discoveries were made [von Huene and Scholl, 1991, Clift and Vannucchi, 2004]. Nowadays, most authors still refer to these early classifications that deserve to be updated, now that we have additional observations.

Another descriptive feature of active margins concerns the amount of sediment available at the trench versus that present between the plate interface and the top of the igneous oceanic crust, that we will further call the “subduction channel”. The thickness of this channel often reflects the erosive or non-erosive behavior of the subduction. Similarly, many authors suggested a causal link between an excess of sediment present in the trench and the generation of mega-earthquakes [Ruff, 1989, Heuret et al., 2012, Scholl et al., 2015].

Even more recently, Lallemand et al. [2018] and van Rijnsingen et al. [2018, 2019] showed that a high ocean floor roughness at 80–100 km wavelengths tended to reduce interseismic coupling on the subduction interface, and hence earthquake magnitude. Seno [2017] was the first to point out that it was not so much the thickness of the sediments at the trench but those actually present in the subduction channel which could condition the seismogenic behavior of the interface. Here, we propose to complete and revise the databases describing active margins from the wealth of work done along subduction zones, in order to verify the assertions made since the 1980s, which were based on a limited number of reference seismic profiles.

Based on a comprehensive review of interpreted seismic profiles published in the literature, we present not only an updated compilation of trench sediment thickness at an unprecedented density but we also provide a first order thickness of the subduction channel on the depth range over which it is imaged. This new database allows us to signifi-

cantly revise the characterization (accretionary versus erosive) of active margins, as well as the solid and fluid fractions of sediment flowing through the subduction channel.

## 2. The NE Japan margin as a case study

Tremendous improvements have been done in the processing of multichannel seismic lines since the 1980’s. It concerns both the penetration depth and the resolution of the data. Figure 1 is an example of the progress made, allowing the NE Japan margin to be imaged with unprecedented accuracy [Park et al., 2021]. The observation of widespread shallow normal faults cutting through the Neogene sedimentary cover of the margin had already been reported [von Huene and Lallemand, 1990] but not their deeper extent. In their interpretation, Park et al. [2021] identified some of these at depths greater than 20 km. Their shallow dip suggests the reactivation of former splay faults into normal faults as similarly observed off Ecuador [Collot et al., 2008] or at the transition from Alaska and Aleutian subduction zones [Kahrizi et al., 2024]. A tiny accretionary wedge (see thrust faults in red in Figure 1), limited to the foot of the margin, reworks the material slid from the margin rather than those deposited in the trench to the extent that the latter is empty of terrigenous deposits. Truncation of margin’s basal reflections along the subduction interface (see green arrow labelled “basal erosion” in Figure 1), seaward deepening of a Miocene subaerial unconformity and sampling of Early Miocene arc volcanic rocks at less than 100 km (see projection of DSDP site 439 in Figure 1) from the present trench attest for subcrustal tectonic erosion since at least 20 Ma [von Huene et al., 1980, von Huene and Lallemand, 1990]. Evidence for landward migration of the volcanic front through time has been reported by Ohguchi et al. [1989]. The >200 km progressive landward migration of the volcanic front is illustrated in the Figure 1 insert. Downdip thickening of the subduction channel primarily observed by von Huene et al. [1994] further north was later observed all along the NE Japan margin [Tsuru et al., 2002]. The thickness of the channel can locally reach up to 3 km–100 km north of the line shown in Figure 1.

Given the progress made and the multitude of seismic lines acquired along the subduction zones since the 1980’s and 1990’s, we have undertaken to

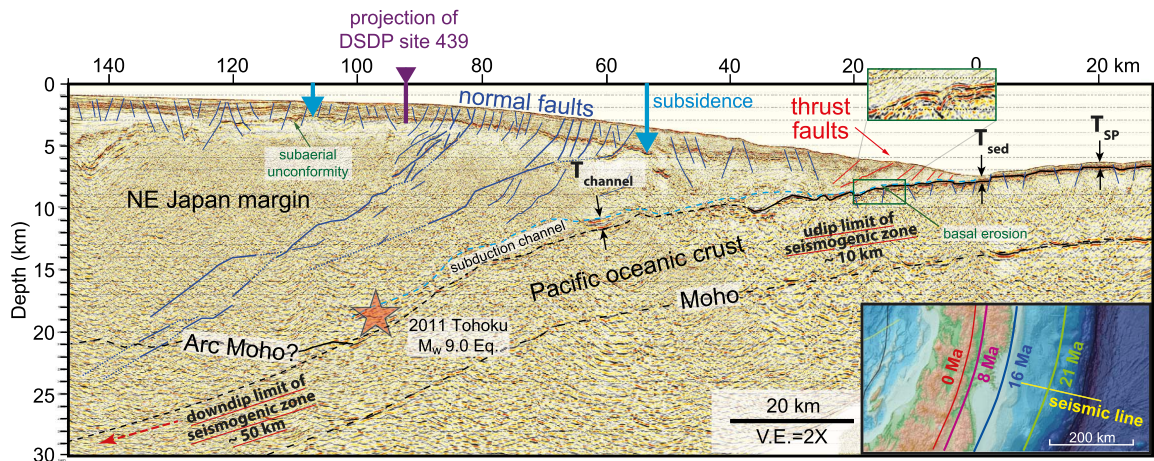


**Figure 1.** Pre-stack depth migrated seismic profile across Japan margin off Ishinomaki Cape modified from Park *et al.* [2021]. Note the extent of normal faults (in dark blue) beyond the Moho, and the restriction of the thrust faults (in red) to the frontal part of the margin. The subduction channel, the top of which is delimited by the dashed pale blue line, is well imaged down to 19 km.  $T_{\text{channel}}$  refers to the thickness of the subduction channel,  $T_{\text{sed}}$  is the trench fill sediment thickness measured at deformation front (maximum thickness) and  $T_{\text{SP}}$  is the average sediment thickness covering the subducting plate away from the trench. Updip and downdip limit of the seismogenic zone based on historical ruptures after Nishikawa *et al.* [2023]. Considering a subduction rate of 92 mm/yr, the subducting oceanic crust near the red star (2011 Tohoku Eq hypocenter) began to underthrust  $\sim 1$  Ma ago. The projection of the DSDP site 439, distant of  $\sim 200$  km from the present-day active volcanic front, where Early Miocene arc volcanic rocks were drilled beneath a subaerial unconformity is shown in purple. Insert: Location of seismic line and volcanic front since 21 Ma after Lallemand [1995].

update the submap database (submap.fr) concerning not only the sediment thickness at the trench  $T_{\text{sed}}$ , but also that of the sediment cover of the lower plate away from the trench  $T_{\text{SP}}$ , and especially that of the subduction channel  $T_{\text{channel}}$  (see Figure 1). On the basis of these elements as well as the morphology of the margin and any additional elements such as the position of the volcanic arc in the past, we were led to revisit the classification of active margins into accretion versus erosion.

### 3. Dominantly accretionary versus erosive margins over the last million years

Sorting active margins into accretionary or erosive types (Figure 2) has long been challenging because the net growth or decrease of the volume of a margin can only be considered over a period that allows the integration of spatial (along and across strike) and

temporal variations, typically from 1 to several million years. Thus, the presence or absence of an active accretionary prism, especially at the margin front, is not sufficient to characterize the margin regime.

For a long time, authors have described the structural complexity of active margins based on the nature of rocks outcropping in the inner forearcs or on seismic reflection images, shedding light on the first  $\sim 10$  km of crust [e.g., Cloos and Shreve, 1988a,b, von Huene and Scholl, 1991]. Thus, the notions of wedge-shaped or channel-like subducted sedimentary units were later imaged, for example, by Tsuru *et al.* [2002] beneath the NE Japan margin. Underplating of sedimentary units that were first underthrust, then incorporated into the margin and ultimately exhumed from large depths as attested by their blueschist and eclogitic facies, was primarily suspected in the Franciscan complex in California [Platt, 1975, Cloos, 1986] and then in numerous ancient accretionary systems [Angiboust *et al.*, 2021].

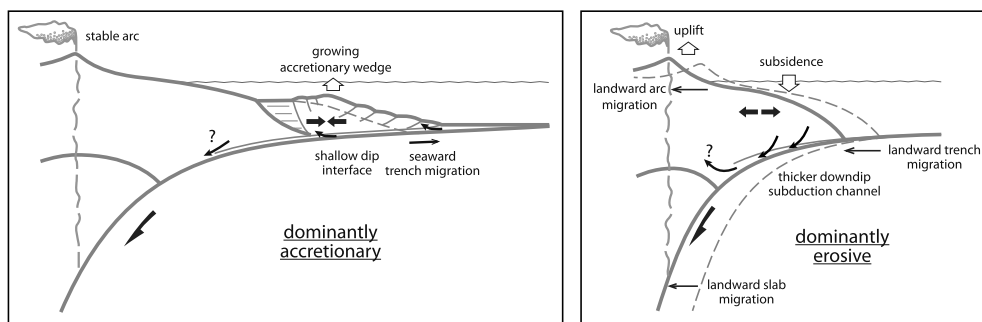


**Figure 2.** Sketch showing two types of active margins. Left: Typical accretionary margin undergoing frontal and subcrustal (underplating) accretion of sediment transferred from the trench or the subduction channel respectively (see small arrows at the base of accretionary wedge). The wedge is growing through time, loading and deflecting the subducting plate (former seafloor in dashed line). The volcanic arc is generally stable with respect to the overlying plate. The tectonic regime is generally compressive. Subcrustal removal may occur (see question mark) so that we prefer to describe this case as dominantly accretionary. Right: Typical erosive margin undergoing frontal and subcrustal tectonic erosion feeding the subduction channel that thickens downdip. The margin is generally narrow because it oversteepens with time, with a maximum of subsidence trenchward, and lacks of significant accretionary wedge. The volcanic arc often migrates landward as the margin shrinks and thins (former seafloor in dashed line). The tectonic regime is generally extensional. Underplating at large depths may happen (see question mark) so that we prefer to describe this case as dominantly erosive.

The detailed exploration of subduction interfaces, such as in Ecuador, Chile or Japan for example [e.g., Collot *et al.*, 2008, Contreras-Reyes *et al.*, 2010, Park *et al.*, 2021], shows that the processes of growth or consumption of the margins evolve in space and time. It is now possible to detect evidence of subcrustal erosion down to depths of 20 km on a seismic profile (Figure 1) and to record uplift in the innermost parts potentially corresponding to the underplating of deeper sedimentary units like in Chile [Angiboust *et al.*, 2021].

von Huene and Scholl [1991] and then Clift and Vannucchi [2004] attempted to estimate the net volume of sedimentary material that is accreted at convergent margins or subducted beneath the basement rocks. The former authors thus classified the margins according to whether or not they are building an accretionary prism while recognizing that the present state does not necessarily reflect the past regime and that visible accretion can mask a deep erosive process. From seismic profiles distributed over 3/4 of the subduction zones, they concluded that 56% of the margins presented an accretionary regime against 44% non-accretionary. The latter authors calculated mass balances for subduction margins

over longer periods—typically >10 m.y.—and then classified the subduction margins into accretionary versus erosive. This had the effect of switching some segments initially identified as accretionary, into erosive segments like Japan, Mexico, Panama, Colombia, Ecuador, N-Peru or Manila. More recently, Festa *et al.* [2018] compiled both classifications by retaining the intent of that of Clift and Vannucchi on the long-term behavior. Noda [2016] proposed a classification of forearc basins based on material transfer between the converging plates like von Huene and Scholl (accretion versus non-accretion) but also on long-term strain field in the basin (compressional versus extensional).

The thickness of sediments observed at a subduction trench  $T_{\text{sed}}$  has been shown to be an important parameter not only in terms of material fluxes [Scholl *et al.*, 1970, von Huene and Scholl, 1991, Clift and Vannucchi, 2004] but also as a parameter that may partly control the seismogenic and tsunamogenic character of the subduction interface, in particular through the fluid content of the subducted section [Ruff, 1989, Le Pichon *et al.*, 1993, Heuret *et al.*, 2012, Scholl *et al.*, 2015, Festa *et al.*, 2018, Brizzi *et al.*, 2018, 2020, Geersen, 2019]. At the same time, many

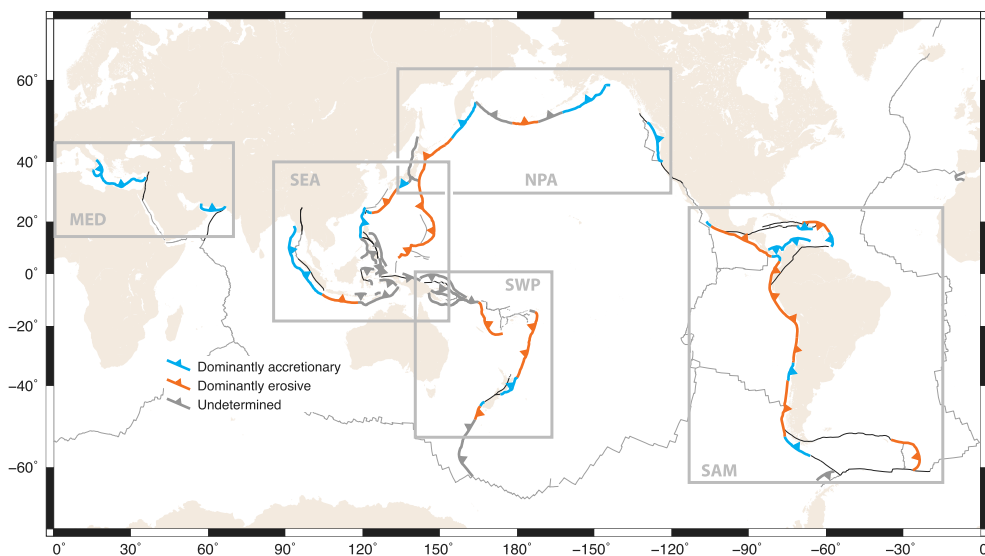


**Figure 3.** Distribution of “dominantly accretionary” (blue trenches) and “dominantly erosive” (red trenches) margins. Grey trenches correspond either to convergent margins where continental crust subducts like north of Australia, or where we do not have enough data to decipher which type is dominant. MED = Mediterranean, SEA = Southeast Asia, NPA = North Pacific, SWP = Southwest Pacific, SAM = South America.

authors pointed out the bias of considering only  $T_{\text{sed}}$  insofar as all or part of the sediments present in the trench could be accreted to the margin and there was ample evidence of material transfer to the margin or to the subduction channel [Heuret *et al.*, 2012, Scholl *et al.*, 2015, Seno, 2017].

The difficulty today, if one wants to test the role of the sedimentary thickness available at the foot of the margin  $T_{\text{sed}}$  or the one effectively dragged into the subduction  $T_{\text{channel}}$ , is to have a reliable database.

Apart from the pioneering work of Ruff [1989] who characterized the 19 margin segments that hosted an earthquake of  $M_w > 8$  according to the presence or absence of an accretionary prism (ETS = Excess Trench Sediment) or horsts and grabens (HGS) on the subducting plate, there are few studies [von Huene and Scholl, 1991, Heuret *et al.*, 2012, Scholl *et al.*, 2015, Seno, 2017], all based on a limited number of observations, then extrapolated.

A close examination of the subduction zones shows that the lateral variations along strike and downdip are sometimes very important. This is why we have undertaken to gather as many observations as possible to upgrade the existing datasets.

Here, we will consider the mid-term behavior (a few m.y.) of the margin based on criteria such as (1) the down-dip variations of the thickness (thickening/thinning) of the subduction channel, (2) the tectonic regime (compressional/extensional) of the margin overriding the subduction interface, (3) its vertical motion (subsidence/uplift), and (4) the migration of the volcanic arc (landward/seaward) (Figure 2). By doing this along 3/4 of the subduction zones, mostly the same as von Huene and Scholl [1991] and Festa *et al.* [2018], we have increased the proportion of dominantly erosive margins (see Table 1 and Figure 3).

## 4. Methodology

### 4.1. Sediment thicknesses estimation

We have (re)analyzed more than 500 multichannel seismic profiles published in 170+ articles covering 88% of the oceanic subduction zones (see Table S1 in Supplementary Material). We still lack precise information for some subduction zones: Solomons,

**Table 1.** Comparison between global classifications of margin types with respective segments lengths (this study)

Trench name	Trench length (km)	von Huene & Scholl (1991) based on the active building (or not) of an accretionary wedge		Clift & Vannuchi (2004) based on mass-balance over ~10 Myrs		Festa & al. (2018) essentially compiled former studies over long periods		This study based on global margin's behavior over few Myrs and MCS data, independent from earlier compilations			Agreement with previous global studies
		accreting	non-accreting	accretionary	erosive	accretionary	erosive	accretionary	erosional	undetermined	
Calabria	600			x		x		600			yes
Aegean-Cyprean	1800	x		x		x		1800			yes
Makran	600	x		x		x		600			yes
Japan	700	x			x		x		700		partly
Kurils - Kamtchatka	2150		x		x	x	x	1250	900		partly
C-W-Aleutians	2300	x		x		x			700	1600	partly
Alaska	1500	x		x		x		1500			yes
Vancouver	400	x		x		x		400			yes
Cascadia	850	x		x		x		850			yes
Central America	3500	x	x		x		x	300	3200		partly
N-Panama	700							700			new
S-Caribbeans	1700							1700			new
Muertos	700							700			new
Hispaniola - PRVI	700		x				x		600	100	yes
Lesser Antilles	1500	x		x		x		500	1000		partly
Colombia	600	x			x		x	200	400		partly
Ecuador	450	x			x		x		450		partly
Peru	2200	x	x		x		x		2200		partly
Chile	4350	x	x	x	x	x	x	1200	3150		partly
S-Sandwich	1100		x		x		x		1100		yes
Andaman	1000	x		x		x		1000			yes
Sumatra	2150	x		x		x		2150			yes
Java	1350	x		x			x		1350		partly
Timor	500	x					x		150	350	partly
Flores	570									570	new
Wetar	350									350	new
Banda incl. Seram	2000									2000	new
Halmahera	700									700	
North Sulawesi	440	x								440	
Sangihe	1300									1300	
East-Luzon	300	x								300	
Philippines	1380		x		x					1380	
Cotobato	380									380	
Sulu	200	x								200	
Manila	1200	x			x	x		1200			partly
Ryukyus incl. W-Gagua	1600		x		x		x	150	1450		partly
Nankai	400	x		x		x		400			yes
Izu-Bonin	1000		x		x		x		1000		yes
Mariana	2400		x		x		x		2400		yes
Yap	600		x						600		yes
Palau	220		x						220		yes
Trobriand	650	x								650	
New Britain	550	x								550	partly
Solomons	1850		x		x					1850	
New Hebrides	1250		x						1250		yes
Tonga	1250		x		x				1250		yes
Kermadec	1500		x		x				1500		yes
Hikurangi	650	x						500	150		partly
Puysegur	500							100	400		new
Macquarie	200		x							200	
Hjort	550									550	
	<b>57390</b>							<b>18500</b>	<b>25420</b>	<b>13470</b>	

Blue (accretion) and red (erosion) trench lengths highlight major changes with respect to earlier classifications.

Halmahera, Philippines, Sulu, Cotobato, Sangihe, N-Sulawesi. Only the data we were able to verify are reported in this study. Instead of providing average values based on one or two profiles, we list mea-

sured values of  $Z_t$ ,  $T_{SP}$ ,  $T_{sed}$  and  $T_{channel}$  line by line even when distant by only few kilometers (see Figures 1 and 4 for definition and Table S1 (Supplementary Material) for access to the complete database).

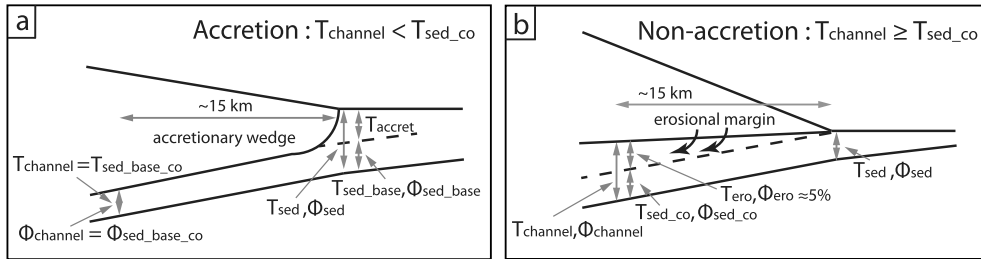


**Figure 4.** The calculation of porosity in the subduction channel at a distance of  $\sim 15$  km from the deformation front is performed differently depending on whether the channel thickness  $T_{\text{channel}}$  is greater or smaller than the  $T_{\text{sed,co}}$  threshold value corresponding to  $T_{\text{sed}} \times K_{\text{co}}$ . If there is frontal accretion, then only the already compacted basal section ( $T_{\text{sed,base}}$ ) of the trench sediments will be entrained, whereas if there is no accretion, the entire  $T_{\text{sed}}$  thickness will be entrained ( $T_{\text{sed,base}} = T_{\text{sed}}$ ). In addition, sediments eroded from the sole of the margin may be added to the subducted section.

Each line, generally normal to the trench, is located by its intersection (latitude, longitude) with the trench.  $Z_t$  is the trench depth in kilometers measured on the seismic line.  $T_{\text{SP}}$  is the average sediment thickness covering the subducting plate away from the trench measured on the seismic line. We do not specify the distance from the deformation front at which we measure  $T_{\text{SP}}$ , as this can vary enormously depending on terrigenous inputs. Our aim is to provide a value for the thickness of the oceanic cover away from the terrigenous inputs that concentrate in the trench. This can be very close to the deformation front if there are no terrigenous inputs, as along most intra-oceanic subduction zones, or several hundred km away if the trench coincides with a detrital fan, as in Cascadia or in the Bay of Bengal.  $T_{\text{sed}}$  is the trench fill sediment thickness measured at deformation front down to the top of the oceanic crust and  $T_{\text{channel}}$  refers to the thickness of the subduction channel between the plate boundary and the top of oceanic crust, close or near the updip limit of the seismogenic zone, as defined for example in Heuret *et al.* [2011]. We will further consider a mean distance of  $\sim 15$  km from the deformation front, given that it may vary from 10 to 30–40 km. As often observed, the thickness of the channel may vary significantly as pore fluids are expelled downdip but also as a function material transfer from or to the margin. This, in conjunction with the fact that the channel imagery is highly variable depending on the quality of the seismic data, especially at great depths (a depth of 20 km, as shown in Figure 1, remains exceptional), means that the

value provided should not be considered as an absolute value but rather as an averaged representative value of the profile. The thicknesses in kilometers are either issued from depth sections or converted from two-way-travel time sections using simplistic empirical laws assuming that sound velocities range from 2 to 3 km/s depending on the thickness for the trench fill sediment. It has sometimes happened that very different values are proposed for sections-depths of the same seismic line in different papers. In this case, we decided after a short investigation which solution made the most sense to us. Again, we do not claim here to provide an exact value that would require knowledge of the seismic velocities on the section-time concerned but an order of magnitude that is close to reality. By doing this, we can reasonably assume an average error between 10 and 20% depending on the quality of the seismic data. The density of the dataset varies greatly from region to region. We extrapolated the margin type to along-strike distances never greater than 200 km when the lateral variations seemed minor. Regarding  $T_{\text{sed}}$  and  $T_{\text{channel}}$ , we did not extrapolate at distances larger than 50 km away from a line. In order to feed the submap database with a step distance of around  $2^\circ$ , we sometimes had to extrapolate the values of  $T_{\text{sed}}$ ,  $T_{\text{channel}}$  and  $T_{\text{SP}}$  along the trenches, based on the nearest measurement, but also on morphological criteria such as the bathymetric profile of the trench. In such case, the symbols of the parameters are then accompanied by an asterisk,  $T_{\text{sed}}^*$ ,  $T_{\text{SP}}^*$ ,  $T_{\text{channel}}^*$ . We provide the source for each seismic line.



#### 4.2. Margin type characterization

The margin type MT “dominantly accretionary” or “dominantly erosive” over the last few million years has been updated (Figures 2 and 3) mainly based on data from the literature but also according to the criteria mentioned in previous section ( $T_{\text{sed}}-T_{\text{channel}}$ , extensional versus compressional regime, margin subsidence/uplift, volcanic front migration).

Raw data set is accessible as supplementary information. Mean values every  $\sim 200$  km of trench are accessible on line at the following url: [submap.fr](http://submap.fr).

#### 4.3. Sediment flux calculation

To estimate the balance of solid or fluid fraction transiting through the subduction channel, we need to estimate the porosity of the sequence in the channel, as well as its thickness. To do this, we convert the depth versus porosity curves of trench floor sedimentary deposits obtained from DSDP and ODP cores and seismic velocities [Figure S1 in Supplementary Material extrapolated in depth from von Huene and Scholl, 1991] into a thickness versus mean porosity curve (Figure S2 in Supplementary Material). Then, we considered 2 distinct cases, depending on whether part of the sedimentary sequence was frontally accreted or not (Figure 4). In the first case (frontal accretion), the channel thickness  $T_{\text{channel}}$  will be less than that of the sedimentary sequence at the trench  $T_{\text{sed}}$  compacted by a factor  $K_{\text{co}}$ , i.e.  $T_{\text{sed\_co}}$ . It means that the incoming section subducting at trench consists only in the lower part of the trench sediment section further called  $T_{\text{sed\_base}}$ . This implies that the mean porosity of the subducting sediment layer  $\Phi_{\text{sed\_base}}$  is less than that of the whole trench sequence, i.e.,  $\Phi_{\text{sed}}$ . The average porosity in the channel  $\Phi_{\text{channel}}$  will be reduced by a factor  $K_r$  compared with that of the subducted section  $\Phi_{\text{sed\_base}}$ . The second case, without frontal accretion, generally corresponds to subcrustal erosion if  $T_{\text{channel}}$  is greater than  $T_{\text{sed\_co}}$ . The channel sequence will therefore be composed of a basal section issued from the trench  $T_{\text{sed\_co}}$  with a porosity  $\theta_{\text{sed\_co}}$ , and an upper section issued from margin removal  $T_{\text{ero}}$  with an average porosity  $\Phi_{\text{ero}} < 10\%$  [Saffer and Tobin, 2011] that we set to 5%. Details of the calculations used to determine an average porosity reduction coefficient  $K_r$  between the incoming section at the trench and the

channel at an average distance of  $\sim 15$  km from the deformation front are given in the Supplementary Material, as well as for the compaction coefficient  $K_{\text{co}}$  between the thickness of incoming sediment and that in the channel. The compaction coefficient  $K_{\text{co}}$  naturally depends on the initial porosity measured at the trench in the incoming sequence, i.e.,  $\Phi_{\text{sed}}$  or  $\Phi_{\text{sed\_base}}$ .

Calculating the solid and fluid fluxes entrained in each subduction zone requires processing the data obtained along the 535 unevenly distributed profiles in such a way as to provide the relevant information per representative transect along each subduction zone. Of the 260 submap database transects, only 116 were able to be assigned with a mean  $T_{\text{channel}}$  value, due to their proximity to a seismic line allowing the channel to be imaged at a distance of at least 10 km from the deformation front. We therefore first estimated the solid and fluid fractions along each of the 116 constrained transects (in green in Table S2 in Supplementary Material) using the estimated porosity  $\Phi_{\text{channel}}$ , and then calculated the fluxes per km of trench by multiplying the solid or liquid fraction by the normal component of the subduction velocity recently updated in the submap database (Table S2). We then extrapolated these values along the subduction zones, weighting them by the width sampled on each transect, which enabled us to cover around 70% of the total length of the subduction zones.

## 5. Results

### 5.1. Margin type

Our updated dataset allowed us to significantly modify the distribution of margin types and, at the end, increase the proportion of “dominantly erosive” margins compared with former studies. We count in this study (see Table 1 and Table S1 in Supplementary Material for details and references) 25,420 km of “dominantly erosive” margins, 18,500 km of “dominantly accretionary” margins and 13,470 km of either undetermined type or where oceanic subduction laterally switches into continental subduction like north of Hispaniola or Australia. In such cases, it is impossible to measure the sediment thickness because the continental basement is either poorly defined or not imaged at all. Based on the 3/4 of subduction zones for which it has been possible

to determine the dominant margin regime, at least in the submerged part, we observe 42% accreting margins (25,420 km) and 58% eroding margins (18,500 km). However, we do not rule out the possibility that some erosive margins may simultaneously record subcrustal accretion far from the deformation front or that some margins assumed to be accreting are subject to deep subcrustal erosion.

We confirm the accretionary character of the Mediterranean, Makran, South Lesser Antilles, Sumatra-Andaman, Alaska, Cascadia, Nankai and South Hikurangi margins (Figure 3). We also confirm the erosional character of the Puerto Rico, South Sandwich, New Hebrides, Izu-Bonin-Mariana or Tonga-Kermadec margins. Some inconsistencies with previous classifications (Table 1) are linked to the time period concerned (current versus 1–2 m.y. versus 10 m.y.). Discrepancy is greatest when von Huene and Scholl [1991] list non-accretionary margins, while we list erosive margins. When re-examining the type of margin, we based our analysis—as indicated above—on a set of criteria and not just on the excess or deficit of sediment present in the subduction channel (see Table 2). The differences with earlier studies include about 600 km of the Lesser Antilles margin north of its intercept with the Tiburon Ridge. The forearc underwent there a dramatic subsidence and extension since middle Miocene (~16 Ma) which is attributed to severe basal erosion following the subduction of the southern extent of the Bahamas Bank [Boucard *et al.*, 2021]. Further west, the Puerto-Rico-Virgin-Islands margin recorded an even stronger episode of tectonic erosion [Grindlay *et al.*, 2005]. Most of the Central America forearc turned into “dominantly erosive” margins [Prada *et al.*, 2023] except the northernmost and southernmost terminations [Bartolomé *et al.*, 2011, MacKay and Moore, 1990]. The Central Aleutians margin is currently considered as accretionary based on the well-developed accretionary wedge but Jicha and Kay [2018] demonstrated that the landward arc migration increased to the west and is greatest over the last 5 m.y. Furthermore, they interpret adakite-like lavas as additional evidence for ongoing subduction-erosion. Northeast Japan and Northern Andes (South Colombia–Ecuador–Peru) turned to exhibit all characters of subduction-erosion even if some local sediment accretion may occur at the margin front [e.g., Collot *et al.*, 2004, Marcaillou *et al.*,

2006]. The Chilean margin shows lateral variations already highlighted in previous classifications, with a predominantly erosive behavior, albeit accretionary evidence in the center. On the other hand, the location of accretionary sectors between 33.4 and 38.2°S and south of 54.1°S is more precise in our study. We agree with Festa *et al.* [2018] that the margin south of Java is dominantly erosive and that the Manila subduction zone is accretionary over its entire length. The Ryukyu margin is still dominantly erosive but we have changed the status of its southernmost termination, between Taiwan and the intersection with the Gagua ridge where sedimentary accretion dominates [Lallemand *et al.*, 2013, Nishizawa *et al.*, 2017]. Finally, we have characterized new margins such as in the Caribbean Sea (North-Panama, South-Caribbeans, Muertos) exhibiting sedimentary accretion or Puysegur south of New Zealand being mainly erosive.

## 5.2. *Total sediment thickness in the trench and the subduction channel*

Based on a re-examination of 500 multichannel seismic lines across the subduction zones, we have updated the database firstly published by Heuret *et al.* [2012] not only regarding the thickness of incoming sediment  $T_{\text{sed}}$  but also those of the subduction channel  $T_{\text{channel}}$  when available as well as those of the sedimentary cover away from the trench area ( $T_{\text{SP}}$ , see Table S1 for data and references line by line). An extract of the database each 2° is provided on the submap web-tool (submap.fr). We have chosen to represent the  $T_{\text{sed}}$  and  $T_{\text{channel}}$  data in visual form with a color code against the margin types (see explanations in Figure 5). The maximum thickness of sediment available in the trench  $T_{\text{sed}}$  is plotted on the ocean side. The thickness of the channel is represented indirectly by subtracting it from the thickness of the sediments in the trench ( $T_{\text{sed}} - T_{\text{channel}}$ ), so that negative values (in red) indicate an excess of subducted sediments over incoming sediments, and positive values (in blue) indicate a deficit of sediments when the upper (or entire) section of entering sediment accrete at the margin front, for example. In absolute terms, knowing that subducted sediments are compacting, it would be necessary to compare  $T_{\text{channel}}$  and  $T_{\text{sed,co}}$ , but as the difference is minor, we have contented ourselves with plotting

**Table 2.** Digest of Table S1 in Supplementary Material

region	trench segments	mean $T_{sed}$	mean $T_{channel}$	mean $T_{sed} - T_{channel}$	compressional vs extensional margin (C,E)	margin's subsidence vs uplift (Su,Up)	evidence for landward volcanic front migration	MT	sources
MED	Calabria	6.4	3.2	3.2	C	Up		accretionary	Gallen <i>et al.</i> (2023)
	Aegean	9.9	4.8	5.1	E	Up		accretionary	Strobl <i>et al.</i> (2014), Gallen <i>et al.</i> (2014)
	Cyprian	9			C	Up		accretionary	Vidal <i>et al.</i> (2000)
MAK	Makran	6.7	3.8	2.9	C	Up		accretionary	Parvatez <i>et al.</i> (2022)
N-PAC	Northeast Japan	0.4	1.4	-1	E	Su	x	erosive	von Huene and Lallemand (1990), Park <i>et al.</i> (2021)
	South Kurils 41.2-46.9°N	0.5	0.5	0	E	Su		erosive	Klaeschen <i>et al.</i> (1994), Schnurle <i>et al.</i> (1995)
	North Kurils - South Kamchatka 47-51°N	0.5	0.5	0	C	Up		accretionary	Klaeschen <i>et al.</i> (1994)
	North Kamchatka	0.7						undetermined	Gribidenko <i>et al.</i> (1983)
	West Aleutians 164-177°E	1.6						erosive	Gribidenko <i>et al.</i> (1983)
	Central Aleutians 179-187.4°E	2	1.4	0.6	C		x	erosive	Baranov <i>et al.</i> (2022), Gribidenko <i>et al.</i> (1983)
	East Aleutians 189-195°E	1.7	1.9	-0.2				undetermined	McCarthy and Scholl (1985), Jicha & Kay (2018)
	West Alaska 197-205°E	1.3	1	0.3	C/E			accretionary	von Huene <i>et al.</i> (2016), Kahrizi <i>et al.</i> (2024)
East Alaska 205-215.5°E	2.5	1.6	0.9	C	Up		accretionary	von Huene and Klaeschen (1999), Fruehn <i>et al.</i> (1999)	
Cascadia	3.3	0.6	2.7	C	Up		accretionary	Davis <i>et al.</i> (1990)	
CARIBBEANS	Central America -20°N	1.1			E			accretionary	Michaud <i>et al.</i> (1996), Bartolomé <i>et al.</i> (2011)
	Central America 8.4-19.1°N	0.6	0.7	-0.1	E	Su		erosive	Aubouin <i>et al.</i> (1984), von Huene and Ranero (2000)
	Central America 6.7-6.8°N	1.3	0.4	0.9	C			accretionary	MacKay and Moore (1990), Silver <i>et al.</i> (1990)
	Panama	2						accretionary	Silver <i>et al.</i> (1990)
	Venezuela	3.2	0.9	2.3	C			accretionary	Kroehler <i>et al.</i> (2011)
	Muertos	1	0.5	0.5	C/E			accretionary	Granja-Bruna <i>et al.</i> (2009, 2014)
	Hispaniola	2.5			C/E			erosive	Rodriguez-Zunero <i>et al.</i> (2020)
	Puerto-Rico	1.9			E	Up/Su		erosive	TenBrink <i>et al.</i> (2005)
	Northern Lesser Antilles 17-20°N	0.5	0.3	0.2	E	Su	x	erosive	Boucard <i>et al.</i> (2021)
	Southern Lesser Antilles 11-16°N	4.4	1.5	2.9	C/E			accretionary	Gomez <i>et al.</i> (2018), Deville (2023)
S-AMERICA	North Colombia 5 - 7°N	0.9	0.4	0.5	C			accretionary	Westbrook <i>et al.</i> (1995)
	Colombia 1.7 - 3.5°N	3.3	1.4	1.9	E	Su		erosive	Collot <i>et al.</i> (2004, 2008)
	Ecuador	0.5	0.5	0	E	Su		erosive	Collot <i>et al.</i> (2004, 2008)
	Peru	0.8	0.8	0	E	Su	x	erosive	von Huene <i>et al.</i> (1989, 1996)
	North Chile 19-33°S	0.4	1	-0.6	E			erosive	Petersen <i>et al.</i> (2021)
	Central Chile 33.4-38.2°S	2	0.9	1.1	C			accretionary	Graveneyr <i>et al.</i> (2003)
	South Chile 39-53°S	1.9	1.7	0.2	C	Up		erosive	Scherwath <i>et al.</i> (2009)
South Chile 54.1-57°S	2.8	1.3	1.5	C/E			accretionary	Polonia <i>et al.</i> (2007)	
Sandwich	0.7			E	Up/Su		erosive	Vanneste and Larter (2002)	
SE-ASIA	Andaman - North Sumatra 1.6 - 14°N	3.7	0.3	3.4	C/E	Up/Su		accretionary	Moeremans <i>et al.</i> (2014), McNeill <i>et al.</i> (2014)
	Sumatra 0 - 8°S	1.5	0.1	1.4	C	Up		accretionary	McNeill <i>et al.</i> (2014)
	Java 105 - 117°E	0.8	0.7	0.1	C			erosive	Kopp (2011)
	Aru	1.4			E	Up		undetermined	Milom <i>et al.</i> (1996)
	Flores	1.2			C	Up		undetermined	Silver <i>et al.</i> (1983)
	Wetar	1			C	Up		undetermined	Silver <i>et al.</i> (1983)
	Seram	1			E			undetermined	Pairault <i>et al.</i> (2003)
	South Manila 14 - 16.7°N	1	0.4	0.6	C	Up		accretionary	Hayes and Lewis (1984)
	North Manila 17 - 24°N	2	0	2	C	Up		accretionary	Ku and Hsu (2009)
	South Ryukyu 122.5 - 123.1°E	4.3	1.1	3.2	C	Up		erosive	Schnurle <i>et al.</i> (1998), Lallemand <i>et al.</i> (1999), Font et Lallemand (2009)
	Ryukyu 124 - 133°E	0.4	0	0.4	C	Su		erosive	Nishizawa <i>et al.</i> (2017), Okamura <i>et al.</i> (2017)
	Nankai	1.6	0.6	1	C	Up		accretionary	Park <i>et al.</i> (2000), Kodaira <i>et al.</i> (2002)
	Izu-Bonin-North Mariana 19 - 33°N	0.3			E	Su	x	erosive	Takahashi <i>et al.</i> (1998)
	Mariana 16.4 - 17.9°N	0.5	0.6	-0.1	E	Su	x	erosive	Oakley <i>et al.</i> (2008)
South Mariana 10.8 - 16.2°N	0.3	0.4	-0.1	E	Su		erosive	Oakley <i>et al.</i> (2008), Ribeiro <i>et al.</i> (2013)	
Yap-Palau	0.2			C/E	Up		erosive	Yang <i>et al.</i> (2018), Dong <i>et al.</i> (2018), Zhang <i>et al.</i> (2019)	
SW-PAC	North New-Hebrides 12 - 17.2°S	1.6	1.6	0	C/E	Up		erosive	Collot <i>et al.</i> (1985, 1992), Fisher <i>et al.</i> (1986, 1991)
	South New-Hebrides 17.5 - 23°S	0.4	1.6	-1.2	E			erosive	Fisher <i>et al.</i> (1986)
	Tonga	0.4	0	0.4	E		x	erosive	Contreras-Reyes <i>et al.</i> (2011), Stratford <i>et al.</i> (2015)
	Kermadec 26.7 - 37.1°S	0.5	0	0.5	E	Su	x	erosive	Funnell <i>et al.</i> (2017), Stratford <i>et al.</i> (2015)
	North Hikurangi 37.8 - 39°S	1.1	0	1.1	C/E	Su		erosive	Scherwath <i>et al.</i> (2010), Gase <i>et al.</i> (2021)
	South Hikurangi 39.1 - 42.3°S	4.4	1	3.4	C	Up		accretionary	Barker <i>et al.</i> (2009), Gase <i>et al.</i> (2021, 2022)
	North Puysegur 45.2 - 45.7°S	2.7	0.4	2.3	C	Up		accretionary	Lebrun <i>et al.</i> (2000), Lamarche et Lebrun (2000)
	South Puysegur 46 - 49°S	1.4	1.2	0.2	C			undetermined	Collot <i>et al.</i> (1995)

Trench segments by region (MED = Mediterranean, MAK = Makran, N-PAC = North Pacific, CARIBBEANS, S-AMERICA = Andes and S-Sandwich, SE-ASIA = Philippine Sea and Sunda, SW-PAC = Southwest Pacific) were firstly defined according to margin type MT, then sediment thickness at trench  $T_{sed}$  and finally sediment thickness below the plate boundary  $T_{channel}$ , each of them showing little variations within a given trench segment. Mean thickness values are reported in km for each segment.

$T_{sed} - T_{channel}$ . As the spacing between seismic profiles is extremely variable from one region to another, from less than 1 km to over 100 km, we plotted the average of  $T_{sed}$  and  $T_{sed}^*$  or  $T_{channel}$  and  $T_{channel}^*$  values as a colored bar every km, perpendicular to the trench, within a sliding window of 100 km along the trench. In other words, empty sectors mean that no values could be measured or estimated at a distance of less than 50 km.

Figure 5 and Table 2 show that we now have an almost complete coverage of  $T_{sed}$  and less coverage of  $T_{channel}$ . Generally speaking, and with rare

exceptions, an excess of sediment in the channel in relation to the thickness of the incoming section highlights the erosive nature of the margin. Positive  $T_{sed} - T_{channel}$  values, reflecting frontal accretion, are sometimes associated with margins with a dominant erosive character (e.g., Central Aleutians 179–187.4°E, Colombia 1.7–3.5°N, North Hikurangi 37.8–39°S). Most of the time, this is due to a bias in  $T_{channel}$  estimation, when its measurement could only be carried out at a short distance from the trench and is not corrected for compaction. For this reason, this value should be used with caution.

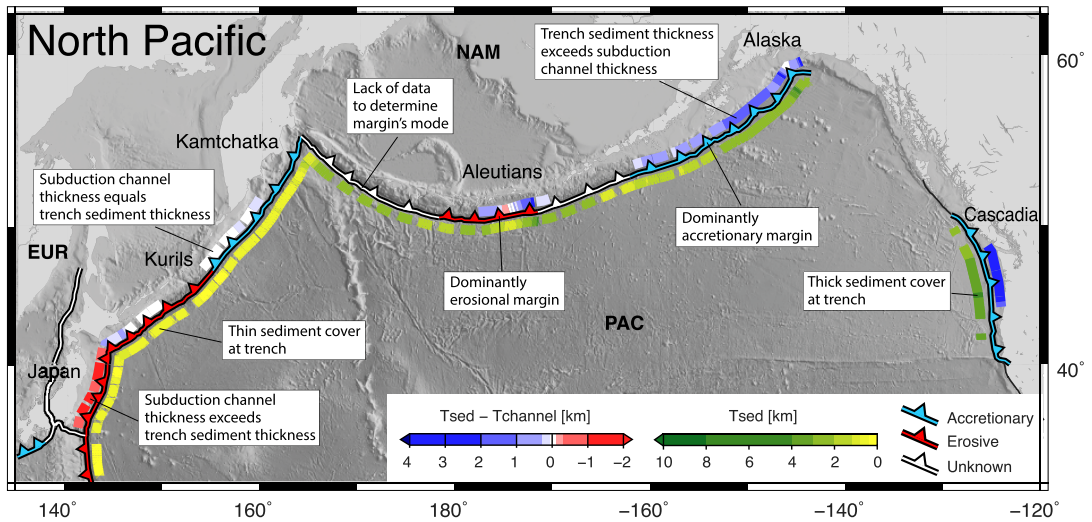


**Figure 5.** Close-up view of margin type and related mean sediment thickness available at trench and within the subduction channel in the North Pacific area. Total sediment thickness in the trench  $T_{sed}$  is plotted in yellow to green colors seaward of the trench axis at the resolution of available MCS data. Landward of the trench axis, we plotted the difference in thickness between the incoming sediments and those of the subduction channel  $T_{sed} - T_{channel}$ . Blue colors mean that the upper part of trench sediment is offscrapped to build the accretionary wedge like off Kamtchatka, whereas red colors mean that the thickness of the subduction channel exceeds those of the entering section like off Tohoku (NE Japan). EUR: Eurasian plate. NAM: North American plate. PAC: Pacific plate.

At the world scale (Figure 6), we observe that thin trench fill, typically less than 0.8 km, often faces erosive margins (South Kuril Islands, NE Japan, Izu-Bonin-Mariana, Ryukyu, Java, Northern Lesser Antilles, Northern Andes, Tonga-Kermadec, New-Hebrides) and thick trench fill, typically more than 0.8 km, often faces accreting margins (Nankai, Manila, Sumatra-Andaman, Alaska, Cascadia, Southern Lesser Antilles, Panama-Venezuela, Hikurangi, Makran or Mediterranean). However, there are some exceptions to this association, such as Northern Kuril-Kamtchatka where accretionary processes may prevail while  $T_{sed}$  does not exceed 0.7 km [Gnibidenko *et al.*, 1983, Klaeschen *et al.*, 1994, Baranov *et al.*, 2022]. We classified the Colombia margin as subject to subduction erosion while mean  $T_{sed}$  between 1.7°N and 3.5°S is 3.3 km and mean  $T_{channel}$  is 1.4 km. According to Collot *et al.* [2008], coeval basal erosion of the outer wedge proceeds pervasively together with deeper underplating with a balance in favor of erosion over the mid-term. Splay faults are activated as new plate boundaries as margin slices are progressively dragged down the

subduction zone. As described above, despite the 2 km sediment thickness in the trench in the central Aleutians between 179 and 187.4°E, the recent landward migration of the arc as well as the composition of the lavas argues for deep tectonic erosion [Jicha and Kay, 2018]. South Chile, between 39 and 53°S, North New-Hebrides, between 12 and 17.2°S, South Puysegur, between 46 and 49°S, Hispaniola and Puerto-Rico combine trench sediment thicknesses more than 1.4 km, thick subduction channels ( $\geq 1.2$  km) and typical characteristics of erosive margins (narrow, steep, sometimes extensional).

We observe large variations of  $T_{sed}$  from one trench to another:  $0.54 \pm 0.4$  km from NE Japan to Kamtchatka,  $1.98 \pm 1.0$  km along the Aleutians-Alaska or  $3.27 \pm 0.5$  km off Cascadia, but also from one profile to the adjacent one, even at short spacing interval like in the central Aleutians for example. Significant local variations in sediment thickness along the trenches are often due to major offsets in the subducting basement, linked to the presence of seamounts or fracture zones, for example.

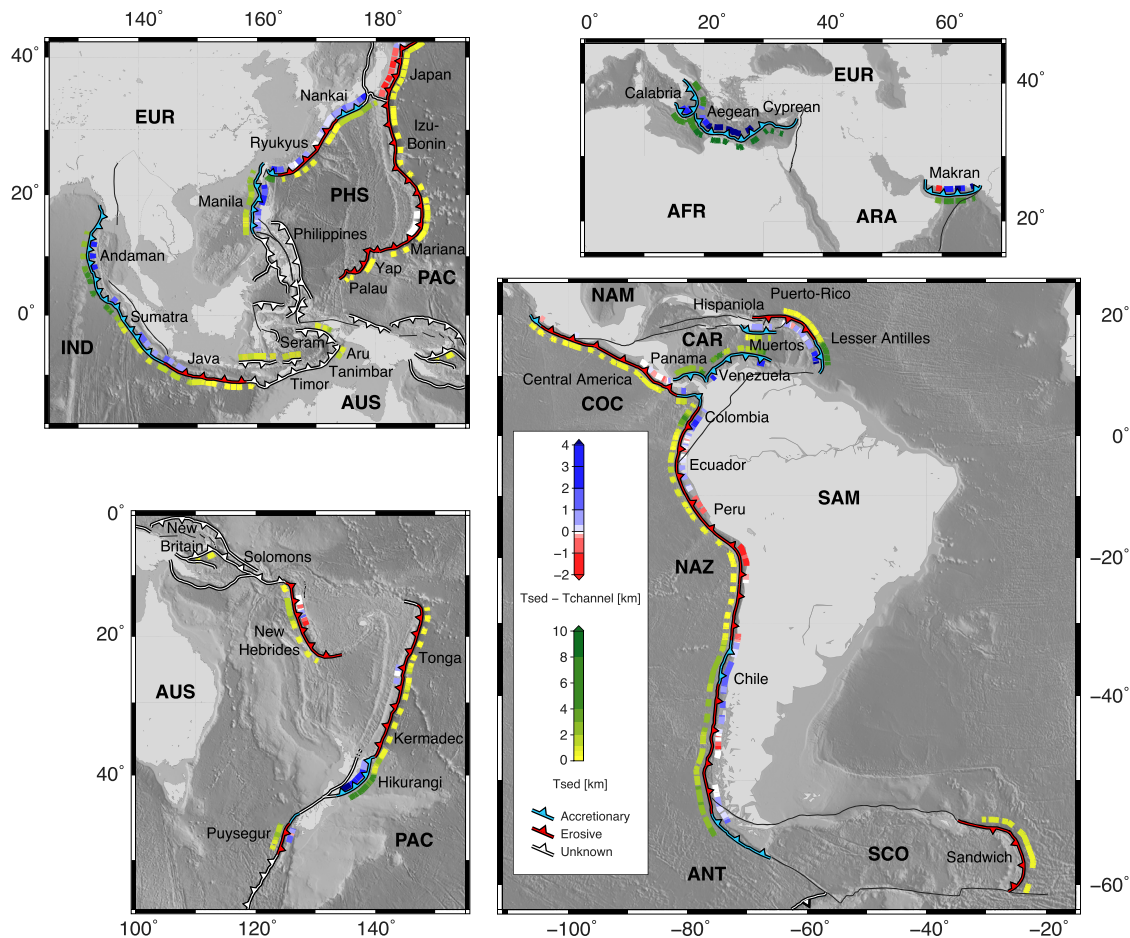


**Figure 6.** Margin type and related mean sediment thickness available at trench and within the subduction channel around the world except the North Pacific area. See also explanations in legend of Figure 5. AFR = Africa plate, ANT = Antarctica plate, ARA = Arabia plate, COC = Cocos plate, IND = India plate, NAZ = Nazca plate, PHS = Philippine Sea plate, SAM = South America plate, SCO = Scotia plate.

### 5.3. Volumes of solid and fluid transiting through the subduction channel

The large number of observations taken along most of the subduction zones enables us to update estimates of solid and fluid fluxes through the subduction channel. In order to compare our results with those proposed by von Huene and Scholl [1991], we attempted to use a similar approach. First, we determined the solid and liquid fraction of the subducted sedimentary section on the basis of average porosity (see Section 4). The major differences, apart from the quantity of data analyzed, consist in measuring the thickness of the channel at an average dis-

tance of  $\sim 15$  km from the deformation front, taking into account compaction in the channel, updating subduction velocities and sometimes differences in trench length (see Supplementary Material for details on the procedure). We then estimated material fluxes per km of trench in areas where we had  $T_{\text{channel}}$  values, and extrapolated these data along the subduction zone. In the absence of constraints on a given subduction zone, such as the Sunda region north of Australia, New Britain and the Solomons, Izu-Bonin, Yap-Palau, Puerto-Rico, Panama, Hjort or South Sandwich, we did not provide estimates. The details of the calculations are provided in the Supplementary material (Table S2) and average porosities

and fluxes values per km of constrained trench and per trench are given in Table 3.

Our results show very strong variations from one subduction zone to another, between sectors where fluxes are gigantic, as in the Aegean, Central America, Chile, New Hebrides and Aleutians, and sectors where fluxes are negligible, as in the Andaman-Sumatra, Ryukyus or Tonga-Kermadec zones. We also note that pore water fluxes are certainly also significant in the same regions where solid fluxes are important, but not in the same proportions. For example, most of the water flowing through the subduction channel is concentrated under Central America, Peru–Chile, and under the New Hebrides, Kuril Islands and Aleutians. In particular, the Aegean subduction zone is characterized by the largest solid flow for a very small fluid flow. On the basis of 70% cumulative trench length, we estimate that every million of years for the past few million years, 1463 km<sup>3</sup> and 396 km<sup>3</sup> of solid sediment and pore water respectively have been transiting through the subduction channel, having subducted some ~15 km from the deformation front. In Table 3, we report the values obtained by von Huene and Scholl [1991], bearing in mind that they only provided solid fluxes based on the porosity of the sediment column estimated at the trench. Surprisingly, in the end, we arrive at the same order of magnitude for solid flux, i.e. 1.5 km<sup>3</sup>/yr along 70% of the subduction zones. In detail, we can see large discrepancies with our estimates (e.g., Aegean, Japan, Central America, Ryukyus, Nankai, New Hebrides, Cascadia, Andaman, Sumatra, Tonga, Kermadec), which can be explained by the smaller number of constrained transects more than 30 years ago, but also by the fact that we have taken into account the first stages of compaction.

## 6. Discussion

### 6.1. $T_{\text{sed}}$ and $T_{\text{channel}}$ may be decorrelated

We have reported the values of Table 2, mean  $T_{\text{sed}}$ , mean  $T_{\text{channel}}$  and margin type MT for each trench segment, on a diagram (Figure 8) after sorting the trench segments, first based on their associated MT and second based on decreasing  $T_{\text{sed}}$ .

Although not all trench segments have information on the thickness of sediment in the subduction

channel, we note that, apart from the major accretionary prisms: Mediterranean, Makran or Southern Lesser Antilles, there is no obvious correspondence or proportionality between the thickness of incoming sediment and that of the channel. However, we note that  $T_{\text{channel}}$  is systematically lower than  $T_{\text{sed}}$  in accreting margins, whereas it is more or less close to  $T_{\text{sed}}$  in eroding margins. This diagram provides information primarily on the thickness of frontally accreted sediment or, on the contrary, the material removed from the prism (subcrustal erosion) that feeds the subduction channel at the front of the prism where it can still be imaged seismically. Even if, overall, the erosive margins are characterized by a small gap between  $T_{\text{sed}}$  and  $T_{\text{channel}}$ , we can see that frontal accretion is carried over along some trench segments, such as in southern Colombia, central Aleutians, Kermadec or the Ryukyus. This means that deep subcrustal erosion of the margin exceeds frontal accretion in these areas.

### 6.2. Porosity variations in the subduction channel

The sediment porosity in the subduction channel  $\Phi_{\text{channel}}$  depends on those of the incoming sequence (beneath the accreted sequence in case of frontal accretion,  $\Phi_{\text{sed\_base}}$ ), a porosity reduction factor  $K_r$ , and the porosity  $\Phi_{\text{ero}}$  of the material subcrustally eroded from the margin (in case of erosion). Assuming  $K_r = 0.85$  and  $\Phi_{\text{ero}} = 5\%$ , it is possible to express  $\Phi_{\text{channel}}$  as a function of  $T_{\text{sed}}$  and  $T_{\text{channel}}$  (see Section 4 and Supplementary Material). Figure 9 shows that maximum porosities are obtained close to the threshold value where  $T_{\text{channel}} = T_{\text{sed\_co}}$  is represented by the straight line. The values obtained on the 116 constrained transects are plotted on the diagram, with triangles representing cases with frontal accretion (below the threshold line) and dots representing cases with erosion (above the threshold line). A wide dispersion can be observed, reflecting the variety of thicknesses in the trench  $T_{\text{sed}}$  as well as those in the channel  $T_{\text{channel}}$ , but on average, porosities are slightly higher for erosive margins, despite the fact that some of the subducted material only has a porosity of 5%. This is because the entire sequence at the trench is subducted under erosive conditions, and the upper part of the sequence at the trench also has the highest porosity.

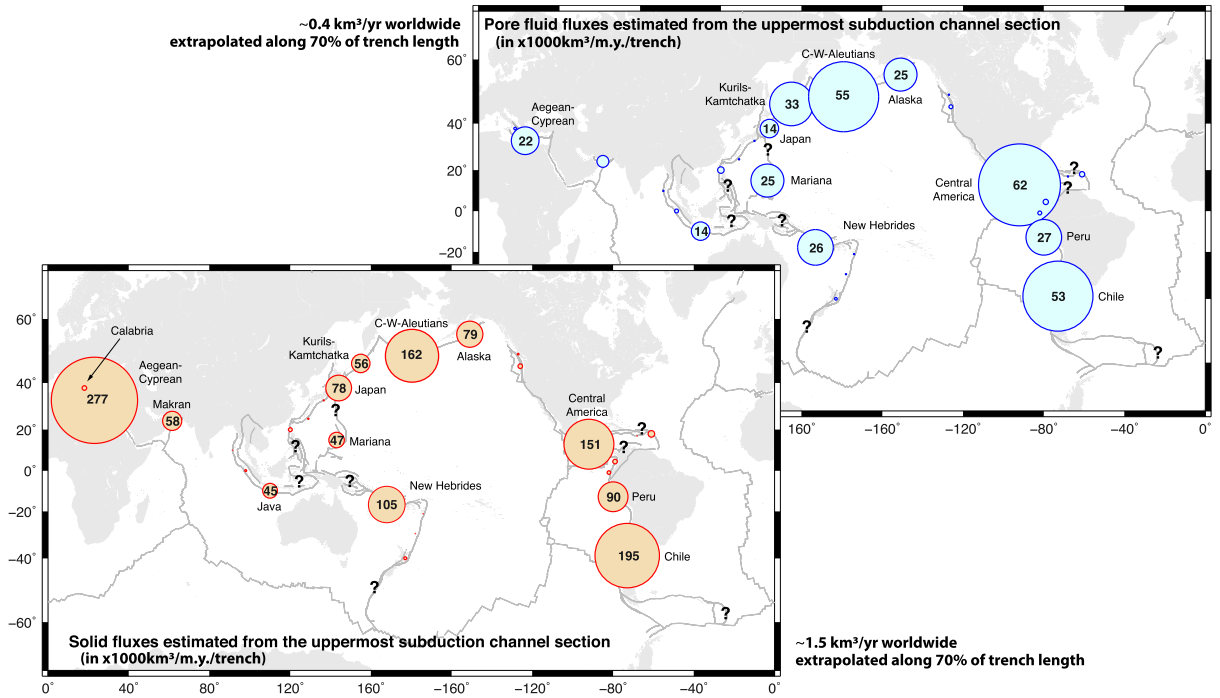


**Figure 7.** Map of solid (sediment) and fluid (pore water) fluxes estimated from the solid and fluid fractions of the subduction channel, having travelled approximately 15 km from the deformation front, by subduction zone in thousands of km<sup>3</sup> per million years.

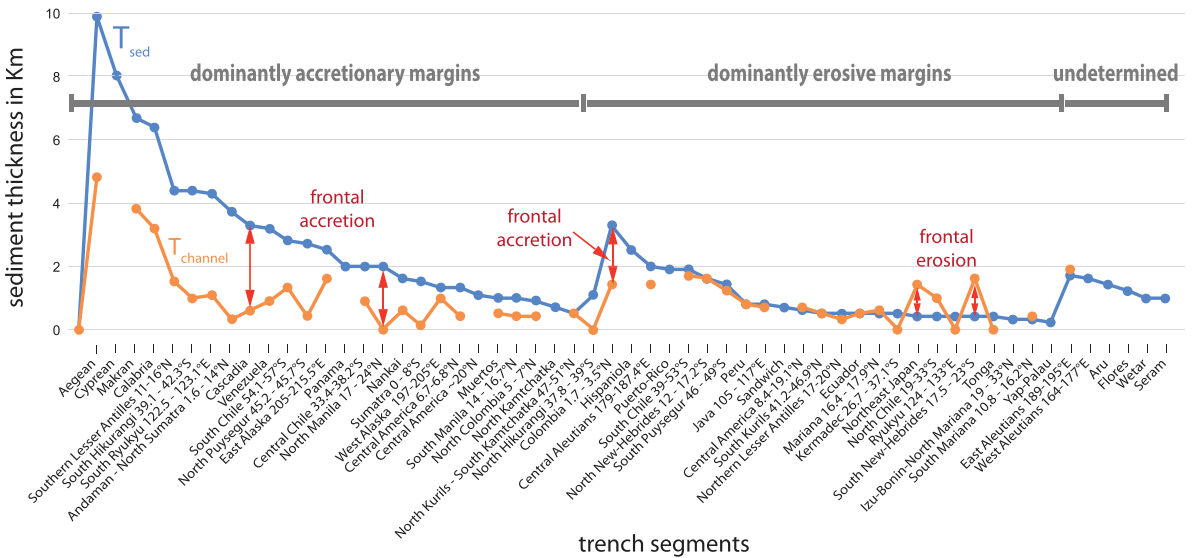


**Figure 8.** Diagram sorting the trench segments first as a function of margin type (grey domains) and second as a function of decreasing  $T_{sed}$  mean values (blue dots and curve). Superimposed are the  $T_{channel}$  mean values (orange) when available. Note that  $T_{channel}$  is often equal or larger than  $T_{sed}$  for dominantly erosive trench segments.

**Table 3.** Mean porosities  $\Phi_{\text{sed}}$  and  $\Phi_{\text{channel}}$  and solid and fluid fluxes dragged into the subduction channel per km of trench and extrapolated per trench

Trench name	Trench length (km)	This study				von Huene & Scholl (1991)				
		Mean porosity in the trench fill at deformation front $\Phi_{\text{sed}}$	Mean porosity in the channel 15 km landward of deformation front $\Phi_{\text{channel}}$	Estimated fraction subducted km <sup>3</sup> /m.y./km of constrained trench	Extrapolated fraction subducted x1000 km <sup>3</sup> /m.y./trench	Estimated fraction subducted km <sup>3</sup> /m.y./km of constrained trench	Extrapolated fraction subducted x1000 km <sup>3</sup> /m.y./trench	Mean porosity in the trench fill at deformation front	Estimated fraction subducted km <sup>3</sup> /m.y./km of trench	Extrapolated fraction subducted x1000 km <sup>3</sup> /m.y./trench
				solid		fluid		solid		
Calabria	600	22.3	13.9	23.6	14.1	4.0	2.4			
Aegean - Cyprian	1800	17.2	7.7	153.9	277.0	12.3	22.1	24.0	66.7	100.0
Makran	600	21.8	12.5	97.4	58.4	14.4	8.6	22.5	113.7	108.0
Japan	700	53.7	15.8	111.4	77.9	20.1	14.1	46.3	36.3	29.0
Kurils - Kamtchatka	2150	50.2	37.3	26.0	56.0	15.3	32.8	40.0	21.8	48.0
C - W-Aleutians	2300	35.1	25.4	70.6	162.5	24.0	55.1			
Alaska	1500	34.8	24.6	52.8	79.1	16.8	25.2	33.0	65.6	177.0
Vancouver	400	29.3	17.3	13.0	5.2	3.3	1.3	33.0	32.5	13.0
Cascadia	850	27.4	17.1	16.9	14.4	3.5	3.0	33.0	37.8	34.0
Central America	3500	47.1	29.5	43.0	150.5	16.9	62.5	43.1	20.0	58.0
N-Panama	700	33.4								
S-Caribbeans	1700	30.3	21.1							
Muertos	700	44.0	30.5	0.7	0.5	0.3	0.2			
Hispaniola - PRVI	700	35.6								
Lesser Antilles	1500	42.7	24.8	13.1	19.6	2.7	4.1	31.0	23.8	19.0
Colombia	600	34.7	22.2	22.6	13.5	5.9	3.5	36.7	53.3	56.0
Ecuador	450	57.1	21.6	25.1	11.3	7.0	3.2			
Peru	2200	48.8	24.9	40.9	90.0	12.5	27.5	42.0	46.7	70.0
Chile	4350	43.8	21.8	44.7	194.5	12.2	53.0	36.7	30.7	135.0
S-Sandwich	1100	45.5						40.0	5.0	4.0
Andaman	1000	29.5		0.0	0.0	0.0	0.0	24.0	80.0	120.0
Sumatra	2150	36.3	28.9	3.0	6.4	1.3	2.7		46.8	96.0
Java	1350	40.7	23.6	33.3	45.0	10.3	13.9	36.7	56.9	37.0
Timor	500									
Flores	570	39.9								
Wetar	350	45.7								
Banda incl. Seram	2000							33.0	46.8	96.0
Halmahera	700									
North Sulawesi	440							42.0	13.3	8.0
Sangihe	1300									
East-Luzon	300									
Philippines	1380	54.8						40.0	21.3	33.0
Cotobato	380									
Sulu	200									
Manila	1200	35.5	27.5	10.3	12.3	4.2	5.0	36.7	6.7	7.0
Ryukyus incl. W-Gagua	1600	47.6	15.3	2.6	4.2	0.5	0.8		14.1	19.0
Nankai	400	38.0	25.2	8.1	3.3	2.7	1.1	36.7	22.5	18.0
Izu-Bonin	1000	57.7						40.0	25.0	25.0
Mariana	2400	55.9	34.9	19.8	47.5	10.5	25.2	40.0	21.7	52.0
Yap	600	60.1						40.0	5.5	3.0
Palau	220	60.1								
Trobriand	650							33.0	21.5	14.0
New Britain	550	44.9						42.0	51.1	46.0
Solomons	1850	53.8						40.0	26.7	28.0
New Hebrides	1250	49.5	23.5	83.8	104.7	20.6	25.8	40.0	23.9	43.0
Tonga	1250	57.7		0.0	0.0	0.0	0.0	40.0	40.7	55.0
Kermadec	1500	54.3		0.0	0.0	0.0	0.0	40.0	17.1	24.0
Hikurangi	650	30.9	13.5	14.4	9.3	2.4	1.6	33.0	31.7	19.0
Puysegur	500	42.5								
Macquarie	200							40.0	6.0	3.0
Hjort	550									
<b>Sums</b>	<b>57390</b>				<b>1457.4</b>		<b>394.6</b>			<b>1597.0</b>

The last 3 columns are values of  $\Phi_{\text{sed}}$  and material fluxes reported from von Huene and Scholl [1991] for comparison, given that the mode of calculations slightly differs (see main text).

### 6.3. Solid and fluid volumes dragged at depth within the subduction channel

Given that we only estimate the volumes of solid or fluid transiting through the shallow subduction

channel, and therefore do not predict transfers between the margin and the subducting plate that may occur deeper down, we have nevertheless updated previous estimates. Our first observation is that  $T_{\text{channel}}$  determines the volume of subducted ma-



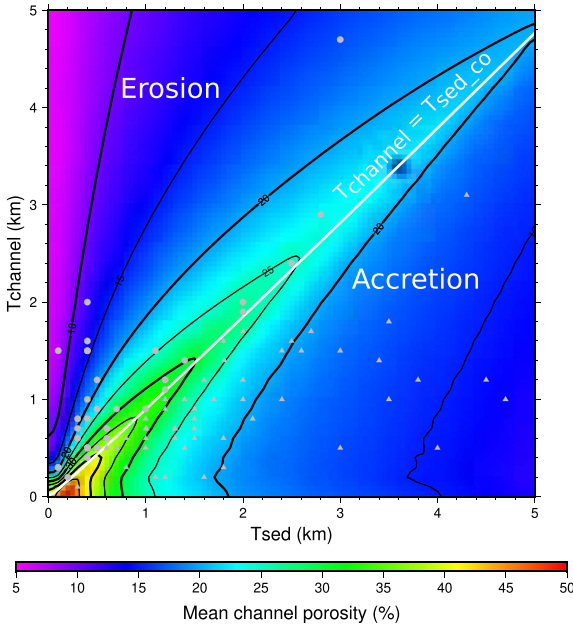


**Figure 9.** Predicted mean porosity in the subduction channel at a distance of  $\sim 15$  km from the deformation front as a function of  $T_{\text{sed}}$  and  $T_{\text{channel}}$ . The dots (erosive margins) and triangles (accretionary margins) represent the values corresponding to the 116 transects for which we have measured both  $T_{\text{channel}}$  and  $T_{\text{sed}}$  (Table S2). We have also drawn the threshold line between frontal accretion and subcrustal erosion when  $T_{\text{channel}} = T_{\text{sed\_co}}$ .

terial, whereas  $T_{\text{sed}}$  will have essentially an effect on  $\Phi_{\text{sed}}$ . Indeed, some subduction zones characterized by thick trench fill like Andaman, Sumatra or Cascadia-Vancouver are associated with very little sediment flux. The reason is that most of the sedimentary pile at trench is accreted frontally. The flux of solid material dragged in depth is decoupled from the subduction rate as illustrated by the Aegean–Cyprean subduction zone which allows the most solid sediment to pass through (Figure 7), while the average subduction rate (normal component) is only 27 mm/yr (Table S2). This is due to the fact that the thickness of the incoming sediments is great (as is the length of the trench), but as a result their porosity is low (17.2%), as they were already compacted before subducting into the channel. As a result, the volume of fluid entrained in this subduc-

tion zone is comparatively very low. Another observation is that the greatest volumes of fluid in the channel globally subduct along erosive margins. This may result from the combination of a larger channel porosity and a higher subduction rate. As indicated above (Section 5), our overall values for subducted solid matter flux are comparable to those estimated by von Huene and Scholl [1991]. In contrast, the volume of subducted fluid is significantly lower in our study, mainly due to the fact that we took into account both the “pre-compaction” of incoming sediments in accretion cases and then applied a porosity reduction factor in the channel. In the end, we obtain  $\sim 0.4$  km<sup>3</sup>/yr of fluids entrained in the channel along 40,450 km of trench, whereas von Huene and Scholl [1991] proposed  $\sim 0.8$  km<sup>3</sup>/yr along 43,450 km of trench.

#### 6.4. $T_{\text{sed}}$ and seismogenic potential along the subduction interface

As we have already pointed out, several studies suggest that subduction mega-earthquakes occur preferentially along opposite sediment-filled trenches [Ruff, 1989, Heuret *et al.*, 2012, Scholl *et al.*, 2015]. Geersen [2019] noted that sediment-starved trenches and rough subducting plates are conducive to tsunami earthquakes. As Geersen, some of the formerly cited authors consider that  $T_{\text{sed}}$  alone is not a good proxy, as the thickness of sediment overlying the subducting plate in the seismogenic zone can sometimes differ quite widely from that available in the trench. Scholl *et al.* [2015], for example, noted the correspondence between most  $M_w \geq 8.5$  earthquakes and high  $T_{\text{sed}}$  values, but pointed out that some  $M_w \geq 8.0$  earthquakes could sometimes occur along weakly sediment-filled trenches facing erosive margins, i.e., the products of subcrustal erosion thicken the subduction channel. Seno [2017] comes to the same conclusion and then provides a rough estimate of the correction to be made to  $T_{\text{sed}}$ . As can be seen, the general idea is that interseismic coupling seems to be stronger with a smooth subduction interface [Lallemand *et al.*, 2018] and a large radius of curvature [Bletery *et al.*, 2016], hence the concern to describe the roughness of this interface as closely as possible. While it remains impossible to image the interface over the entire depth range of the seismogenic zone, we provide here an estimate of

$T_{\text{channel}}$  close or at the updip limit of the seismogenic zone [ $\sim 11 \pm 4$  km in average according to Heuret *et al.*, 2011] in a number of regions. The analysis of this new dataset with the objective to evaluate and eventually revisit our former conclusions based on a less complete dataset is under process.

### 6.5. *Nature of the incoming sediment*

It is not just the thickness of the sediments in the trench or channel that is important, but recent studies show that their nature and spatial distribution are likely to play a role in seismogenic potential. It appears that the mud-rich mass transport deposits (MTDs) modify the architecture and properties of the subduction channel [Festa *et al.*, 2018, Geersen *et al.*, 2020]. Heterogeneous fabric and fluid content possibly favor slow ruptures, particularly in shallow parts. Magmatic intrusions (sills) within the sedimentary cover appear as patches in few areas around the rupture area of the 2011 Tohoku earthquake. Fujie *et al.* [2020] thus suggest that disturbance and thermal metamorphism associated with this recent volcanic activity modify and shape the size and distribution of interplate earthquakes off NE Japan. In the Nankai subduction zone, Park and Jamali Hondori [2023] suggest that the underthrust turbidites cause low pore-fluid overpressure and high effective vertical stress across the décollement inhibiting the slow earthquakes occurrence. Similar heterogeneities were also found in the shallow part of the subduction interface along the Hikurangi margin [Gase *et al.*, 2022]. There, they consist of pelagic carbonates versus heterogeneous volcanoclastics. The presence of pelagic carbonates above thickened non-volcanic siliciclastic sediments plays a key role in smoothing the rough topography of the subducting plate and higher coupling that could be prone to large ruptures. In this study, we do not directly address the question of the nature of the incoming sediments, as this would require lengthy developments, but we provide whenever possible a proxy for the contribution of terrigenous inputs via the submarine drainage network thanks to the difference between  $T_{\text{sed}}$  and  $T_{\text{SP}}$  (Table S1). Unsurprisingly, we find the great detrital fans such as the Nile in the Mediterranean, the Indus or Bengal in the Makran and Andaman, the Astoria and Nitinat in the Cascades or the Orinoco in the Lesser Antilles.

### 6.6. *Uncertainties on plate interface transient migration*

Mass transfer occurs in the vicinity of the plate boundary landward of the deformation front from the subducting to the overriding plate (underplating) or the opposite (basal erosion). By nature, field evidences of erosive structures in the vicinity of exhumed subduction channels are tiny [Bachmann *et al.*, 2009, Vannucchi *et al.*, 2010]. Such a mass transfer process assumes that the subduction interface migrates upwards pervasively via hydrofracturing of the overriding plate sole [e.g., von Huene *et al.*, 2004] or transiently in the wake of a seamount, for example [e.g., Lallemand *et al.*, 1994]. Similarly, certain discontinuities along the interface, such as variations in fluid pressure or rheology, can cause downward migration of the décollement, leading to the incorporation of a subduction channel slice at the margin [underplating, Sample and Moore, 1987, von Huene and Scholl, 1991, Raimbourg *et al.*, 2019, Angiboust *et al.*, 2021]. Today, it is relatively easy to trace the décollement at shallow levels, based on seismic reflection amplitudes and polarity reversals. Sometimes, we can observe the ghosts of abandoned paleo-décollements such as in the Nankai accretionary wedge [deep strong reflector of Park *et al.*, 2002]. Based on the estimates of basal versus internal friction along the Chilean margin, Cubas *et al.* [2022] were able to characterize the sectors of the subduction interface where deformation was distributed, i.e. where forethrusts paralleled the interface. The authors interpret this type of condition (small differences in friction) as favorable to underplating, but it could just as easily favor basal erosion. The distribution of the deformation around the plate interface over the last Ma makes analysis (margin type,  $T_{\text{channel}}$ ) complex on the basis of the current image of the margin alone.

## 7. Conclusion

We provide in this study an exhaustive database describing the lateral variations of the sediment thickness covering the oceanic plate when approaching a subduction zone, at the deformation front in the trench and in the shallow portion (<20 km) of the subduction channel. The unprecedented density of the data acquired opens the door to future

multivariate analyses, notably concerning the dependence of the seismogenic behavior of the subduction interface on the thickness of the subduction channel versus that of the sediments present in the trench. A mass balance of material transfer from the trench to depths through the subduction channel, as proposed by von Huene and Scholl [1991], is updated by analyzing fluxes, knowing the convergence rate and making assumptions on the sediment porosity, over the last m.y. Maximum porosity in the channel is reached when there is no accretion or tectonic erosion.

With the caveat that the observations used to carry out this study can be traced back to the last m.y., while the seismic lines or morphology reflect the current to recent state, and the vertical motions of the margin or the migration of the volcanic arc incorporates a longer period, we propose an adjustment in the tectonic style of certain margins, with a final erosive dominance.

### Dedication

The first author would like to dedicate this study to Roland von Huene, Jean Aubouin's partner at a time when the process of subcrustal tectonic erosion of active margins had only just been revealed and was the subject of much criticism.

### Declaration of interests

The authors do not work for, advise, own shares in, or receive funds from any organization that could benefit from this article, and have declared no affiliations other than their research organizations.

### Acknowledgements

We are grateful to Jin-Oh Park who kindly provided us the seismic line of Figure 1. We would like to thank Hugues Raimbourg for his detailed review, and in particular his encouragement to revisit material balance on the basis of our new data. We would also like to thank the anonymous reviewer. Finally, the first author is particularly grateful to one of the co-editors of this special issue, Laurent Jolivet, for prompting him to update his knowledge of a subject that first attracted his attention some thirty years ago.

### Supplementary data

Supporting information for this article is available on the journal's website under <https://doi.org/10.5802/crgeos.252> or from the author.

### References

- Angiboust, S., Menant, A., Gerya, T., and Oncken, O. (2021). The rise and demise of deep accretionary wedges: A long-term field and numerical modeling perspective. *Geosphere*, 17(X), 1–35.
- Aubouin, J., Bourgois, J., and Azéma, J. (1984). A new type of active margin: the convergent-extensional margin, as exemplified by the Middle America trench off Guatemala. *Earth Planet. Sci. Lett.*, 67(2), 211–218.
- Aubouin, J., Bourgois, J., and Azéma, J. (1985). Two types of active margins: convergent-compressional margins and convergent-extensional margins. In Nasu, N. et al., editors, *Formation of Active Ocean Margins*, pages 109–129. TERRAPUB, Tokyo.
- Bachmann, R., Oncken, O., Glodny, J., Seifert, W., Georgieva, V., and Sudo, M. (2009). Exposed plate interface in the European Alps reveals fabric styles and gradients related to an ancient seismogenic coupling zone. *J. Geophys. Res.*, 114, 1–23.
- Baranov, B. V., Tsukanov, N. V., Gaedicke, C., Freitag, R., and Dozorova, K. A. (2022). Morphology and structural features of the subduction zone in the vicinity of Kuril–Kamchatka–Aleutian junction. *Oceanology*, 62(4), 528–539.
- Barker, D. H. N., Sutherland, R., Henrys, S., and Bannister, S. (2009). Geometry of the Hikurangi subduction thrust and upper plate, North Island, New Zealand. *Geochem. Geophys. Geosyst.*, 10(2), article no. Q02007.
- Bartolomé, R., Danobeitia, J., Michaud, F., Cordoba, D., and Delgado-Argote, L. A. (2011). Imaging the seismic crustal structure of the Western Mexican margin between 19°N and 21°N. *Pure Appl. Geophys.*, 168, 1373–1389.
- Bletery, Q., Thomas, A. M., Rempel, A. W., Karlstrom, L., Sladen, A., and De Barros, L. (2016). Mega-earthquakes rupture flat megathrusts. *Science*, 354(6315), 1027–1031.

- Bloomer, S. H. (1983). Distribution and origin of igneous rocks from the landward slopes of the Mariana Trench: Implications for its structure and evolution. *J. Geophys. Res.*, 88, 7411–7428.
- Boucard, M., Marcaillou, B., Lebrun, J.-F., Laurencin, M., Klingelhoefer, F., Laigle, M., Lallemand, S., Schenini, L., Graindorge, D., Cornée, J.-J., Münch, P., Philippon, M., and the AntiTheSis and GARAnti Scientific teams (2021). Paleogene V-shaped basins and Neogene subsidence of the Northern Lesser Antilles forearc. *Tectonics*, 40, article no. e2020TC006524.
- Brizzi, S., Sandri, L., Funicello, E., Corbi, E., Piro-mallo, C., and Heuret, A. (2018). Multivariate statistical analysis to investigate the subduction zone parameters favoring the occurrence of giant megathrust earthquakes. *Tectonophysics*, 728–729, 92–103.
- Brizzi, S., van Zelst, I., Funicello, E., Corbi, E., and van Dinther, Y. (2020). How sediment thickness influences subduction dynamics and seismicity. *J. Geophys. Res.: Solid Earth*, 125, article no. e2019JB018964.
- Clift, P. and Vannucchi, P. (2004). Controls on tectonic accretion versus erosion in subduction zones: Implications for the origin and recycling of the continental crust. *Rev. Geophys.*, 42(2), article no. RG2001.
- Cloos, M. (1986). Blueschists in the Franciscan Complex of California: Petrotectonic constraints on uplift mechanisms. In *Blueschists and Eclogites*, Geological Society of America Memoir, 164, pages 77–93. Geological Society of America.
- Cloos, M. and Shreve, R. L. (1988a). Subduction-channel model of prism accretion, melange formation, sediment subduction, and subduction erosion at convergent plate margins: 1. Background and description. *Pure Appl. Geophys.*, 128(3/4), 455–500.
- Cloos, M. and Shreve, R. L. (1988b). Subduction-channel model of prism accretion, melange formation, sediment subduction, and subduction erosion at convergent plate margins: 1. Implications and discussion. *Pure Appl. Geophys.*, 128(3/4), 501–545.
- Collot, J.-Y., Agudelo, W., Ribodetti, A., and Marcaillou, B. (2008). Origin of a crustal splay fault and its relation to the seismogenic zone and underplating at the erosional north Ecuador–south Colombia oceanic margin. *J. Geophys. Res.*, 113, article no. B12102.
- Collot, J. Y., Daniel, J., and Burne, R. V. (1985). Recent tectonics associated with the subduction/collision of the d'Entrecasteaux zone in the central New Hebrides. *Tectonophysics*, 112(1–4), 325–356.
- Collot, J. Y., Lallemand, S., Pelletier, B., Bissen, J. P., Glaçon, G., Fisher, M. A., Greene, H. G., Boulin, J., Daniek, J., and Monzier, M. (1992). Geology of the d'Entrecasteaux-New Hebrides Arc collision zone: results from a deep submersible survey. *Tectonophysics*, 212(3–4), 213–241.
- Collot, J. Y., Lamarche, G., Wood, R. A., Delteil, J., Sosson, M., Lebrun, J. F., and Coffin, M. F. (1995). Morphostructure of an incipient subduction zone along a transform plate boundary: Puységur Ridge and Trench. *Geology*, 23(6), 519–522.
- Collot, J.-Y., Marcaillou, B., Sage, F., Michaud, F., Agudelo, W., Charvis, P., Graindorge, D., Gutscher, M.-A., and Spence, G. (2004). Are rupture zone limits of great subduction earthquakes controlled by upper plate structures? Evidence from multichannel seismic reflection data acquired across the northern Ecuador–southwest Colombia margin. *J. Geophys. Res.*, 109, article no. B11103.
- Contreras-Reyes, E., Flueh, E. R., and Grevemeyer, I. (2010). Tectonic control on sediment accretion and subduction off south central Chile: Implications for coseismic rupture processes of the 1960 and 2010 megathrust earthquakes. *Tectonics*, 29, article no. TC6018.
- Contreras-Reyes, E., Grevemeyer, I., Watts, A. B., Flueh, E. R., Peirce, C., Moeller, S., and Papenberg, C. (2011). Deep seismic structure of the Tonga subduction zone: Implications for mantle hydration, tectonic erosion, and arc magmatism. *J. Geophys. Res.: Solid Earth*, 116(B10), article no. B10103.
- Cubas, N., Agard, P., and Tissandier, R. (2022). Earthquake ruptures and topography of the Chilean margin controlled by plate interface deformation. *Solid Earth*, 13(3), 779–792.
- Davis, E. E., Hyndman, R. D., and Villinger, H. (1990). Rates of fluid expulsion across the Northern Cascadia Accretionary Prism: Constraints from new heat flow and multichannel seismic reflection data. *J. Geophys. Res.: Solid Earth*, 95(B6), 8869–8889.
- Deville, E. (2023). Dynamics of brittle-viscous accretionary wedges as revealed by geophysical and drilling data and analog modeling of

- the Barbados prism. *Tectonics*, 42(10), article no. e2023TC007851.
- Dong, D., Zhang, Z., Bai, Y., Fan, J., and Zhang, G. (2018). Topographic and sedimentary features in the Yap subduction zone and their implications for the Caroline Ridge subduction. *Tectonophysics*, 722, 410–421.
- Ferrière, J. and Faure, M. (2024). Jean Aubouin et les chaînes de montagnes: des observations aux synthèses. L'itinéraire scientifique d'un géologue au rayonnement international. *C. R. Géosci.*, 356(S2), 1–19. (this issue).
- Festa, A., Dilek, Y., Mittempergher, S., Ogata, K., Pini, G. A., and Remitti, F. (2018). Does subduction of mass transport deposits (MTDs) control seismic behavior of shallow-level megathrusts at convergent margins? *Gondwana Res.*, 60, 186–193.
- Fisher, M. A. (1986). Tectonic processes at the collision of the d'Entrecasteaux zone and the New-Hebrides island arc. *J. Geophys. Res.: Solid Earth*, 91(B10), 10470–10486.
- Fisher, M. A., Collot, J. Y., and Geist, E. L. (1991). The collision zone between the North d'Entrecasteaux Ridge and the New Hebrides Island Arc: 2. Structure from multichannel seismic data. *J. Geophys. Res.: Solid Earth*, 96(B3), 4479–4495.
- Font, Y. and Lallemand, S. (2009). Subducting oceanic high causes compressional faulting in southernmost Ryukyu forearc as revealed by hypocentral determinations of earthquakes and reflection/refraction seismic data. *Tectonophysics*, 466(3–4), 255–267.
- Fruehn, J., von Huene, R., and Fisher, M. A. (1999). Accretion in the wake of terrane collision: The Neogene accretionary wedge off Kenai Peninsula, Alaska. *Tectonics*, 18(2), 263–277.
- Fujie, G., Kodaira, S., Nakamura, Y., Morgan, J. P., Dannowski, A., Thorwart, M., Grevemeyer, I., and Miura, S. (2020). Spatial variations of incoming sediments at the northeastern Japan arc and their implications for megathrust earthquakes. *Geology*, 48, 614–619.
- Funnell, M. J., Peirce, C., and Robinson, A. H. (2017). Structural variability of the Tonga-Kermadec forearc characterized using robustly constrained geophysical data. *Geophys. J. Int.*, 210(3), 1681–1702.
- Gallen, S. F., Seymour, N. M., Glotzbach, C., Stockli, D. E., and O'Sullivan, P. (2023). Calabrian forearc uplift paced by slab–mantle interactions during subduction retreat. *Nat. Geosci.*, 16, 513–520.
- Gallen, S. F., Wegmann, K. W., Bohnenstiehl, D. R., Pazzaglia, F. J., Brandon, M. T., and Fassoulas, C. (2014). Active simultaneous uplift and margin-normal extension in a forearc high, Crete, Greece. *Earth Planet. Sci. Lett.*, 398, 11–24.
- Gase, A. C., Bangs, N. L., van Avendonk, H. J. A., Bassett, D., and Henrys, S. A. (2022). Hikurangi megathrust slip behavior influenced by lateral variability in sediment subduction. *Geology*, 50(10), 1145–1149.
- Gase, A. C., Van Avendonk, H. J., Bangs, N. L., Bassett, D., Henrys, S. A., Barker, D. H., Kodaira, S., Jacobs, K. M., Luckie, T. W., Okaya, D. A., Fujie, G., Yamamoto, Y., Arnulf, A. F., and Arai, R. (2021). Crustal structure of the northern Hikurangi margin, New Zealand: Variable accretion and overthrusting plate strength influenced by rough subduction. *J. Geophys. Res.: Solid Earth*, 126(5), article no. e2020JB021176.
- Geersen, J. (2019). Sediment-starved trenches and rough subducting plates are conducive to tsunami earthquakes. *Tectonophysics*, 762(2019), 28–44.
- Geersen, J., Festa, A., and Remitti, F. (2020). Structural constraints on the subduction of mass transport deposits in convergent margins. In Georgiopoulou, A., Amy, L. A., Benetti, S., Chaytor, J. D., Clare, M. A., Gamboa, D., Haughton, P. D. W., Moernaut, J., and Mountjoy, J. J., editors, *Subaqueous Mass Movements and their Consequences: Advances in Process Understanding, Monitoring and Hazard Assessments*, Geological Society, London, Special Publications, 500, pages 115–128. Geological Society of London.
- Gnibidenko, H., Bykova, T. G., Veselov, O. V., Vorobiev, V. M., and Svarichevsky, A. S. (1983). The tectonics of the Kuril-Kamchatka deep-sea trench. In Hilde, T. W. C. and Uyeda, S., editors, *Geodynamics of the Western Pacific-Indonesian Region*, volume 11 of *AGU Series*, pages 249–286. American Geophysical Union, Washington, DC.
- Gomez, S., Bird, D., and Mann, P. (2018). Deep crustal structure and tectonic origin of the Tobago-Barbados ridge. *Interpretation*, 6(2), T471–T484.
- Granja-Bruña, J., Carbó-Gorosabel, A., Estrada, P. L., Muñoz Martín, A., Ten Brink, U. S., Gomez Ballesteros, M., Druet, M., and Pazos, A. (2014). Morphostructure at the junction between the Beata ridge and the Greater Antilles island arc (offshore

- Hispaniola southern slope). *Tectonophysics*, 618, 138–163.
- Granja Bruña, J. L., Ten Brink, U. S., Carbó-Gorosabel, A., Muñoz-Martín, A., and Ballesteros, M. G. (2009). Morphotectonics of the central Muertos thrust belt and Muertos Trough (northeastern Caribbean). *Mar. Geol.*, 263(1–4), 7–33.
- Grevemeyer, I., Díaz-Naveas, J. L., Ranero, C. R., Villinger, H. W., and Leg, O. D. P. (2003). Heat flow over the descending Nazca plate in central Chile, 32 S to 41 S: Observations from ODP Leg 202 and the occurrence of natural gas hydrates. *Earth Planet. Sci. Lett.*, 213(3–4), 285–298.
- Grindlay, N. R., Mann, P., Dolan, J. F., and van Gestel, J.-P. (2005). Neotectonics and subsidence of the northern Puerto-Rico-Virgin Islands margin in response to the oblique subduction of high-standing ridges. In Mann, P., editor, *Active Tectonics and Seismic Hazards of Puerto-Rico, the Virgin Islands, and Offshore Areas*, Geological Society, London, Special Publications, 385, pages 31–60. Geological Society of London.
- Hayes, D. E. and Lewis, S. D. (1984). A geophysical study of the Manila Trench, Luzon, Philippines: 1. Crustal structure, gravity, and regional tectonic evolution. *J. Geophys. Res.: Solid Earth*, 89(B11), 9171–9195.
- Heuret, A., Conrad, C., Funicello, F., Lallemand, S., and Sandri, L. (2012). Relation between subduction megathrust earthquakes, trench sediment thickness and upper plate strain. *Geophys. Res. Lett.*, 39(5), article no. L05304.
- Heuret, A., Lallemand, S., Funicello, F., Piromallo, C., and Faccenna, C. (2011). Physical characteristics of subduction interface type seismogenic zones revisited. *Geochem. Geophys. Geosyst.*, 12, article no. Q01004.
- Jicha, B. R. and Kay, S. M. (2018). Quantifying arc migration and the role of forearc subduction erosion in the central Aleutians. *J. Volcanol. Geotherm. Res.*, 360, 84–99.
- Kahrizi, A., Delescluse, M., Chamot-Rooke, N., Pubellier, M., Bécel, A., Shillington, D., Nedimovic, M., and Bulois, C. (2024). Extensional forearc structures at the transition from Alaska to Aleutian Subduction Zone: slip partitioning, terranes and large earthquakes. *C. R. Géosci.*, 356(S2), 1–25. (this issue).
- Klaeschen, D., Belykh, I., Gnibidenko, H., Patrikeyev, S., and von Huene, R. (1994). Structure of the Kuril trench from seismic reflection records. *J. Geophys. Res.*, 99(B12), 24173–24188.
- Kodaira, S., Kurashimo, E., Park, J. O., Takahashi, N., Nakanishi, A., Miura, S., Iwasaki, T., Hirata, N., Ito, K., and Kaneda, Y. (2002). Structural factors controlling the rupture process of a megathrust earthquake at the Nankai trough seismogenic zone. *Geophys. J. Int.*, 149(3), 815–835.
- Kopp, H. (2011). The Java convergent margin: structure, seismogenesis and subduction processes. *Geol. Soc., Lond., Spec. Publ.*, 355(1), 111–137.
- Kroehler, M. E., Mann, P., Escalona, A., and Christeson, G. L. (2011). Late Cretaceous-Miocene diachronous onset of back thrusting along the South Caribbean deformed belt and its importance for understanding processes of arc collision and crustal growth. *Tectonics*, 30(6), article no. TC6003.
- Ku, C. Y. and Hsu, S. K. (2009). Crustal structure and deformation at the northern Manila Trench between Taiwan and Luzon islands. *Tectonophysics*, 466(3–4), 229–240.
- Lallemand, S., Liu, C. S., Dominguez, S., Schnürle, P., and Malavieille, J. (1999). Trench-parallel stretching and folding of forearc basins and lateral migration of the accretionary wedge in the southern Ryukyus: A case of strain partition caused by oblique convergence. *Tectonics*, 18(2), 231–247.
- Lallemand, S., Peyret, M., van Rijsingen, E., Arcay, D., and Heuret, A. (2018). Roughness characteristics of oceanic seafloor prior to subduction in relation to the seismogenic potential of subduction zones. *Geochem. Geophys. Geosyst.*, 19, 2121–2146.
- Lallemand, S., Theunissen, T., Schnürle, P., Lee, C. S., Liu, C. S., and Font, Y. (2013). Indentation of the Philippine Sea plate by the Eurasia plate in Taiwan: Details from recent marine seismological experiments. *Tectonophysics*, 594, 60–79.
- Lallemand, S. E. (1995). High rates of arc consumption by subduction processes: some consequences. *Geology*, 6, 551–554.
- Lallemand, S. E., Schnürle, P., and Malavieille, J. (1994). Coulomb theory applied to accretionary and nonaccretionary wedges: Possible causes for tectonic erosion and/or frontal accretion. *J. Geophys. Res.: Solid Earth*, 99(B6), 12033–12055.
- Lamarche, G. and Lebrun, J. F. (2000). Transition from strike-slip faulting to oblique subduction: active tectonics at the Puysegur Margin, South New

- Zealand. *Tectonophysics*, 316(1–2), 67–89.
- Le Pichon, X., Henry, P., and Lallemand, S. (1993). Accretion and erosion in subduction zones: The role of fluids. *Annu. Rev. Earth Planet. Sci.*, 21, 307–331.
- Lebrun, J. F., Lamarche, G., Collot, J. Y., and Delteil, J. (2000). Abrupt strike-slip fault to subduction transition: The Alpine fault-Puysegur trench connection, New Zealand. *Tectonics*, 19(4), 688–706.
- MacKay, M. E. and Moore, G. F. (1990). Variation in deformation of the South Panama accretionary prism: response to oblique subduction and trench sediment variation. *Tectonics*, 9(4), 683–698.
- Marcaillou, B., Spence, G., Collot, J.-Y., and Wang, K. (2006). Thermal regime from bottom simulating reflectors along the north Ecuador–south Colombia margin: Relation to margin segmentation and great subduction earthquakes. *J. Geophys. Res.*, 111, article no. B12407.
- McCarthy, J. I. L. L. and Scholl, D. W. (1985). Mechanisms of subduction accretion along the central Aleutian Trench. *Geol. Soc. Am. Bull.*, 96(6), 691–701.
- McNeill, L. C. and Henstock, T. J. (2014). Forearc structure and morphology along the Sumatra-Andaman subduction zone. *Tectonics*, 33(2), 112–134.
- Michaud, F., Mercier De Lepinay, B., Bourgois, J., and Calmus, T. (1996). Evidence for active extensional tectonic features within the Acapulco trench fill at the Rivera-North America plate boundary. *C. R. Acad. Sci., Sér. 2*, 323(2), 145–152.
- Milsom, J., Kaye, S., and Sardjono, S. (1996). Extension, collision and curvature in the eastern Banda arc. *Geol. Soc., Lond., Spec. Publ.*, 106(1), 85–94.
- Moeremans, R., Singh, S. C., Mukti, M., McArdle, J., and Johansen, K. (2014). Seismic images of structural variations along the deformation front of the Andaman–Sumatra subduction zone: implications for rupture propagation and tsunamigenesis. *Earth Planet. Sci. Lett.*, 386, 75–85.
- Moore, G. F., Shipley, T. H., and Lonsdale, P. F. (1986). Subduction erosion versus sediment off-scraping at the toe of the Middle America trench off Guatemala. *Tectonics*, 5(4), 513–523.
- Natland, J. and Tarney, J. (1981). Petrologic evolution of the Mariana arc and back-arc basin system—a synthesis of drilling results in the South Philippine Sea. *Init. Rep. DSDP*, 60, 877–908.
- Nishikawa, T., Ide, S., and Nishimura, T. (2023). A review on slow earthquakes in the Japan Trench. *Progr. Earth Planet. Sci.*, 10(1), 1–51.
- Nishizawa, A., Kaneda, K., Oikawa, M., Horiuchi, D., Fujioka, Y., and Okada, C. (2017). Variations in seismic velocity distribution along the Ryukyu (Nansei-Shoto) Trench subduction zone at the northwestern end of the Philippine Sea plate. *Earth Planet. Space*, 69, article no. 86.
- Noda, A. (2016). Forearc basins: Types, geometries, and relationships to subduction zone dynamics. *Geol. Soc. Am. Bull.*, 128(5/6), 879–895.
- Oakley, A. J., Taylor, B., and Moore, G. F. (2008). Pacific Plate subduction beneath the central Mariana and IzuBonin fore arcs: New insights from an old margin. *Geochem. Geophys. Geosyst.*, 9(6), article no. Q06003.
- Ohguchi, T., Yoshida, T., and Okami, K. (1989). Historical change of the Neogene and Quaternary volcanic field in the northeast Honshu arc. In Kitamura, N. et al., editors, *Cenozoic Geotectonics of Northeast Honshu Arc*, Geological Society of Japan Memoir, 32, pages 431–455. Geological Society of Japan. (in Japanese with English abstract).
- Okamura, Y., Nishizawa, A., Oikawa, M., and Horiuchi, D. (2017). Differential subsidence of the forearc wedge of the Ryukyu (Nansei-Shoto) Arc caused by subduction of ridges on the Philippine Sea Plate. *Tectonophysics*, 717, 399–412.
- Pairault, A. A., Hall, R., and Elders, C. F. (2003). Structural styles and tectonic evolution of the Seram Trough, Indonesia. *Mar. Petrol. Geol.*, 20(10), 1141–1160.
- Park, J. O. and Jamali Hondori, E. (2023). Link between the Nankai underthrust turbidites and shallow slow earthquakes. *Sci. Rep.*, 13(1), article no. 10333.
- Park, J.-O., Tsuru, T., Fujie, G., Jamali Hondori, E., Kagoshima, T., Takahata, N., Zhao, D., and Sano, Y. (2021). Seismic reflection images of possible mantle-fluid conduits and basal erosion in the 2011 Tohoku earthquake rupture area. *Front. Earth Sci.*, 9, article no. 687382.
- Park, J. O., Tsuru, T., Kodaira, S., Nakanishi, A., Miura, S., Kaneda, Y., and Kono, Y. (2000). Out-of-sequence thrust faults developed in the coseismic slip zone of the 1946 Nankai earthquake (Mw = 8.2) off Shikoku, southwest Japan. *Geophys. Res. Lett.*, 27(7), 1033–1036.
- Park, J. O., Tsuru, T., Takahashi, N., Hori, T., Kodaira,

- S., Nakanishi, A., Miura, S., and Kaneda, Y. (2002). A deep strong reflector in the Nankai accretionary wedge from multichannel seismic data: Implications for underplating and interseismic shear stress release. *J. Geophys. Res.: Solid Earth*, 107(B4), article no. ESE-3.
- Parvaiz, S., Ali, A., Javed, F., and Shah, M. A. (2022). Deformational pattern and seismogenic potential of the eastern Makran subduction zone. *J. Asian Earth Sci.*, 235, article no. 105298.
- Petersen, F., Lange, D., Ma, B., Grevemeyer, I., Geersen, J., Klaeschen, D., Contreras-Reyes, E., Barrientos, S., Tréhu, A. M., Vera, E., and Kopp, H. (2021). Relationship between subduction erosion and the updip limit of the 2014 Mw 8.1 Iquique earthquake. *Geophys. Res. Lett.*, 48(9), article no. e2020GL092207.
- Platt, J. P. (1975). Metamorphic and deformational processes in the Franciscan Complex, California: Some insights from the Catalina Schist terrane. *Geol. Soc. Am. Bull.*, 86, 1337–1347.
- Polonia, A., Torelli, L., Brancolini, G., and Loreto, M. F. (2007). Tectonic accretion versus erosion along the southern Chile trench: Oblique subduction and margin segmentation. *Tectonics*, 26(3), article no. TC3005.
- Prada, M., Bartolomé, R., Gras, C., Bandy, W. L., and Danobeitia, J. J. (2023). Trench-parallel ridge subduction controls upper-plate structure and shallow megathrust seismogenesis along the Jalisco-Colima margin, Mexico. *Commun. Earth Environ.*, 4, article no. 53.
- Raimbourg, H., Famin, V., Palazzin, G., Yamaguchi, A., Augier, R., Kitamura, Y., and Sakaguchi, A. (2019). Distributed deformation along the subduction plate interface: The role of tectonic mélanges. *Lithos*, 334–335, 69–87.
- Ranero, C. R. and von Huene, R. (2000). Subduction erosion along the Middle America convergent margin. *Nature*, 404(6779), 748–752.
- Ribeiro, J. M., Stern, R. J., Martinez, F., Ishizuka, O., Merle, S. G., Kelley, K., Anthony, E. Y., Ren, M., Ohara, Y., Reagan, M., Girard, G., and Bloomer, S. (2013). Geodynamic evolution of a forearc rift in the southernmost Mariana Arc. *Isl. Arc*, 22(4), 453–476.
- Rodríguez-Zurrunero, A., Granja-Bruña, J. L., Muñoz-Martín, A., Leroy, S., ten Brink, U., Gorosabel-Araus, J. M., Gomez de la Pena, L., Druet, M., and Carbó-Gorosabel, A. (2020). Along-strike segmentation in the northern Caribbean plate boundary zone (Hispaniola sector): Tectonic implications. *Tectonophysics*, 776, article no. 228322.
- Ruff, L. (1989). Do trench sediments affect great earthquake occurrence in subduction zones? *Pure Appl. Geophys.*, 129, 263–282.
- Rutland, R. (1971). Andean orogeny and ocean floor spreading. *Nature*, 233, 252–255.
- Saffer, D. M. and Tobin, H. J. (2011). Hydrogeology and mechanics of subduction zone forearcs: Fluid flow and pore pressure. *Annu. Rev. Earth Planet. Sci.*, 39, 157–186.
- Sample, J. C. and Moore, J. C. (1987). Structural style and kinematics of an underplated slate belt, Kodiak and adjacent islands, Alaska. *Geol. Soc. Am. Bull.*, 99, 7–20.
- Scherwath, M., Contreras-Reyes, E., Flueh, E. R., Grevemeyer, I., Krabbenhöft, A., Papenberg, C., Petersen, C. J., and Weinrebe, R. W. (2009). Deep lithospheric structures along the southern central Chile margin from wide-angle P-wave modelling. *Geophys. J. Int.*, 179(1), 579–600.
- Scherwath, M., Kopp, H., Flueh, E. R., Henrys, S. A., Sutherland, R., Stagpoole, V. M., Barker, D. H. N., Reyners, M. E., Bassett, D. G., Planert, L., and Danowski, A. (2010). Forearc deformation and underplating at the northern Hikurangi margin, New Zealand. *J. Geophys. Res.: Solid Earth*, 115(B6), article no. B06408.
- Schnürle, P., Lallemand, S. E., von Huene, R., and Klaeschen, D. (1995). Tectonic regime of southern Kurile trench as revealed by multichannel seismic lines. *Tectonophysics*, 241(3–4), 259–278.
- Schnürle, P., Liu, C. S., Lallemand, S. E., and Reed, D. L. (1998). Structural insight into the south Ryukyu margin: Effects of the subducting Gagua Ridge. *Tectonophysics*, 288(1–4), 237–250.
- Scholl, D., Christensen, M., von Huene, R., and Marlow, M. (1970). Peru–Chile trench sediments and sea-floor spreading. *Geol. Soc. Am. Bull.*, 81(5), 1339–1360.
- Scholl, D. W., Kirby, S. H., von Huene, R., Ryan, H., Wells, R. E., and Geist, E. L. (2015). Great ( $\geq$  Mw8.0) megathrust earthquakes and the subduction of excess sediment and bathymetrically smooth seafloor. *Geosphere*, 11(2), 236–265.
- Seely, D. (1979). Geophysical investigations of continental slopes and rises. In Watkins, J. S., Mon-



- tadert, L., and Dickerson, P. W., editors, *Geological and Geophysical Investigations of Continental Margins*, volume 29, pages 245–260. American Association of Petroleum Geologists.
- Seno, T. (2017). Subducted sediment thickness and Mw 9 earthquakes. *J. Geophys. Res.: Solid Earth*, 122, 470–491.
- Silver, E. A., Reed, D., McCaffrey, R., and Joyodiwiryo, Y. (1983). Back arc thrusting in the eastern Sunda arc, Indonesia: A consequence of arc-continent collision. *J. Geophys. Res.: Solid Earth*, 88(B9), 7429–7448.
- Silver, E. A., Reed, D. L., Tagudin, J. E., and Heil, D. J. (1990). Implications of the north and south Panama thrust belts for the origin of the Panama orocline. *Tectonics*, 9(2), 261–281.
- Stratford, W., Peirce, C., Paulatto, M., Funnell, M., Watts, A. B., Grevemeyer, I., and Bassett, D. (2015). Seismic velocity structure and deformation due to the collision of the Louisville Ridge with the Tonga-Kermadec Trench. *Geophys. J. Int.*, 200(3), 1503–1522.
- Strobl, M., Hetzel, R., Fassoulas, C., and Kubik, P. W. (2014). A long-term rock uplift rate for eastern Crete and geodynamic implications for the Hellenic subduction zone. *J. Geodyn.*, 78, 21–31.
- Suess, E., von Huene, R., et al. (1988). Ocean Drilling Program Leg 112, Peru continental margin: Part 2, Sedimentary history and diagenesis in a coastal upwelling environment. *Geology*, 16(10), 939–943.
- Takahashi, N., Suyehiro, K., and Shinohara, M. (1998). Implications from the seismic crustal structure of the northern Izu–Bonin arc. *Isl. Arc*, 7(3), 383–394.
- Ten Brink, U. (2005). Vertical motions of the Puerto Rico Trench and Puerto Rico and their cause. *J. Geophys. Res.: Solid Earth*, 110(B6), article no. B06404.
- Tsuru, T., Park, J.-O., Miura, S., Kodaira, S., Kido, Y., and Hayashi, T. (2002). Along-arc structural variation of the plate boundary at the Japan Trench margin: Implication of interplate coupling. *J. Geophys. Res.*, 107(B12), article no. 2357.
- van Rijsingen, E., Funicello, F., Corbi, F., and Lallemand, S. (2019). Subduction interface roughness affects the occurrence of megathrust earthquakes: insights from analog models. *Geophys. Res. Lett.*, 46, 3124–3132.
- van Rijsingen, E., Lallemand, S., Peyret, M., Arcay, D., Heuret, A., Funicello, F., and Corbi, F. (2018). How subduction interface roughness influences the occurrence of large interplate earthquakes. *Geochem. Geophys. Geosyst.*, 19(8), 2342–2370.
- Vanneste, L. E. and Larter, R. D. (2002). Sediment subduction, subduction erosion, and strain regime in the northern South Sandwich forearc. *J. Geophys. Res.: Solid Earth*, 107(B7), article no. EPM-5.
- Vannucchi, P., Remitti, F., Bettelli, G., Boschi, C., and Dallai, L. (2010). Fluid history related to the early Eocene-middle Miocene convergent system of the Northern Apennines (Italy): Constraints from structural and isotopic studies. *J. Geophys. Res.*, 115, 1–23.
- Vidal, N., Alvarez-Marrón, J., and Klaeschen, D. (2000). The structure of the Africa–Anatolia plate boundary in the eastern Mediterranean. *Tectonics*, 19(4), 723–739.
- von Huene, R. and Aubouin, J. (1982). Summary—Leg 67, Middle America Trench transect off Guatemala. In Aubouin, J., von Huene, R., et al., editors, *Init. Rep. DSDP*, volume 67, pages 775–793. Washington, DC, US Government Printing Office.
- von Huene, R., Aubouin, J., Azéma, J., Blackinton, G., Carter, J., Coulbourn, W., Cowan, D., Curiale, J., Dengo, C., Faas, R., et al. (1980). Leg 67—The Deep-Sea Drilling Project Mid-America trench transect off Guatemala. *Geol. Soc. Am. Bull.*, 91(7), 421–432.
- von Huene, R., Bourgois, J., Miller, J., and Pautot, G. (1989). A large tsunamogenic landslide and debris flow along the Peru Trench. *J. Geophys. Res.: Solid Earth*, 94(B2), 1703–1714.
- von Huene, R. and Klaeschen, D. (1999). Opposing gradients of permanent strain in the aseismic zone and elastic strain across the seismogenic zone of the Kodiak shelf and slope, Alaska. *Tectonics*, 18(2), 248–262.
- von Huene, R., Klaeschen, D., Cropp, B., and Miller, J. (1994). Tectonic structure across the accretionary and erosional parts of the Japan Trench margin. *J. Geophys. Res.: Solid Earth*, 99(B11), 22349–22361.
- von Huene, R. and Lallemand, S. (1990). Tectonic erosion along convergent margins;. *Geol. Soc. Am. Bull.*, 102, 704–720.
- von Huene, R., Langseth, M., Nasu, N., and Okada, H. (1982). A summary of Cenozoic tectonic history along the IPOD Japan Trench transect. *Geol. Soc. Am. Bull.*, 93(9), 829–846.
- von Huene, R., Miller, J. J., and Dartnell, P. (2016). A possible transoceanic tsunami directed toward

- the US west coast from the Semidi segment, Alaska convergent margin. *Geochem. Geophys. Geosyst.*, 17(3), 645–659.
- von Huene, R., Pecher, I. A., and Gutscher, M. A. (1996). Development of the accretionary prism along Peru and material flux after subduction of Nazca Ridge. *Tectonics*, 15(1), 19–33.
- von Huene, R., Ranero, C. R., and Vannucchi, P. (2004). Generic model of subduction erosion. *Geology*, 32(10), 913–916.
- von Huene, R. and Scholl, D. (1991). Observations at convergent margins concerning sediment subduction, subduction erosion, and the growth of continental crust. *Rev. Geophys.*, 29(3), 279–316.
- Westbrook, G. K., Hardy, N. C., and Heath, R. P. (1995). Structure and tectonics of the Panama-Nazca plate boundary. In Mann, P., editor, *Geologic and Tectonic Development of the Caribbean Plate Boundary in Southern Central America*, Geological Society of America Special Paper, 295, pages 91–112. Geological Society of America, Boulder, CO.
- Yang, Y., Wu, S., Gao, J., Tian, L., Yang, J., and Xu, Y. (2018). Geology of the Yap Trench: new observations from a transect near 10°N from manned submersible Jiaolong. *Int. Geol. Rev.*, 60(16), 1941–1953.
- Zhang, Z. Y., Dong, D. D., Sun, W. D., Wu, S. G., Bai, Y. L., Wang, X. J., and Fan, J. K. (2019). Subduction erosion, crustal structure, and an evolutionary model of the northern Yap subduction zone: New observations from the latest geophysical survey. *Geochem. Geophys. Geosyst.*, 20(1), 166–182.